

Dynamic parameterized quantum circuits: expressive and barren-plateau free

Abhinav Deshpande¹, Marcel Hinsche^{2,3}, Sona Najafi^{4,5}, Kunal Sharma⁴, Ryan Sweke¹, and Christa Zoufal²

¹IBM Quantum, Almaden Research Center, San Jose, California 95120, USA

²IBM Quantum, IBM Research Europe – Zurich

³Dahlem Center for Complex Quantum Systems, Freie Universität Berlin, Germany

⁴IBM Quantum, IBM T.J. Watson Research Center, Yorktown Heights, 10598, USA

⁵MIT-IBM Watson AI Lab, Cambridge MA, 02142, USA

Abstract

Classical optimization of parameterized quantum circuits is a widely studied methodology for the preparation of complex quantum states, as well as the solution of machine learning and optimization problems. However, it is well known that many proposed parameterized quantum circuit architectures suffer from drawbacks which limit their utility, such as the hardness of optimization due to their classical simulability or a problem known as “barren plateaus”. We propose and study a class of *dynamic* parameterized quantum circuit architectures. These are parameterized circuits containing intermediate measurements and feedforward operations. In particular, we show that these architectures:

1. Provably do not suffer from barren plateaus.
2. Are expressive enough to describe arbitrarily deep unitary quantum circuits.
3. Are competitive with state of the art methods for the preparation of ground states and facilitate the representation of nontrivial thermal states.

These features make the proposed architectures promising candidates for a variety of applications.

Contents

1	Introduction	3
1.1	Structure of this work	3
1.2	Our results and contributions	4
1.2.1	Dynamic parameterized quantum circuits	4
1.2.2	Expressivity	5
1.2.3	Absence of barren plateaus	5
1.2.4	Numerical results	7
1.2.5	Classical simulability	8
2	Variational quantum algorithms	8
3	Dynamic parameterized quantum circuit architectures	10
3.1	Dynamic quantum circuits	10
3.2	Dynamic parameterized quantum circuit architecture proposals	11
3.3	Relation to existing nonunitary architectures	13
4	Trainability	14
4.1	What does it mean for a PQC architecture to be trainable?	14
4.2	Barren plateaus	15
4.3	Absence of barren plateaus in dynamic parameterized quantum circuits	16
4.4	The stat-mech model	17
4.5	A unified derivation of barren plateaus from the stat-mech model	17
4.6	Gradient evaluation	18
5	Potential utility	19
5.1	Ground state preparation	19
5.2	Thermal state preparation	22
5.3	Caveats and criticisms	24
6	Classical hardness	25
6.1	Worst-case hardness	26
6.2	Average-case hardness (easiness)	27
6.3	Do hard instances occur during optimization?	28
7	Outlook and conclusions	30
Appendix		31
A	Definitions and Notation	31
B	The stat-mech model	33
B.1	Connection between the stat-mech model and barren plateaus	37
B.2	Stat-mech mapping rules for circuits with feedforward operations	39
B.3	Physics of the feedforward stat-mech model	41

1 Introduction

Variational quantum algorithms (VQAs) are a broad class of highly studied quantum algorithms for solving a diverse range of problems [Cer+21a]. Specifically, there are now VQA based approaches for machine learning with classical data [BLSF19], classical optimization [Zho+20], learning quantum systems [Car+23] and the preparation of ground and thermal states of complex quantum systems [Til+22; Cer+21a]. The basic idea of all variational quantum algorithms is as follows: one defines a class of parameterized quantum circuits, chooses an initial circuit structure from this class in some way, and then iteratively updates the circuit parameters or circuit structure using a classical optimization algorithm. This iterative adjustment seeks to minimize a cost function, which is designed to evaluate the quality of a specific quantum circuit as a solution to the problem at hand.

Given the above, the first thing one needs to do when designing a variational quantum algorithm is choose an appropriate parameterized quantum circuit (PQC). At a high level, any good PQC for a specific problem should ideally satisfy all of the following criteria:

1. **Expressivity:** There should exist circuit parameter instances which correspond to good solutions to the problem of interest.
2. **Trainability:** One should be able to find the circuit instances corresponding to good solutions, via the chosen optimization method, using a polynomial amount of resources such as measurements and time.
3. **Classical hardness:** There should not exist a classical algorithm that can efficiently simulate the PQC, and hence, the variational algorithm.

While a large variety of different PQC architectures have been proposed, there are unfortunately not many candidates which might satisfy all three criteria. In fact, it is not even clear how to rigorously formalize each criterion [GGPD24], or whether it is indeed possible to satisfy all three simultaneously for meaningful problems. More specifically, for a large variety of architectures there is a known tradeoff between expressivity and trainability. In particular, one can show that expressivity often leads to “barren plateaus”, which are an obstacle to trainability via gradient-based optimization algorithms [Lar+24]. Often, this tradeoff also leads to another impediment. In particular, one can also show that for a wide variety of architectures, decreasing expressivity sufficiently to mitigate barren plateaus can often lead to the existence of efficient algorithms for classical simulations [Cer+23].

With this in mind, in this work we study *dynamic* parameterized quantum circuits and argue that they help tackle the tradeoff between expressivity and trainability. In doing so, we are free to restore expressivity, making these circuits classically hard to simulate in the worst case. Specifically, we study parameterized quantum circuits that include nonunitary measurement and feedforward operations, which are known to provide a significant resource for quantum error correction [ABIN96], measurement-based quantum computing [Bri+09], and the preparation of interesting states [MSWC24; Bäu+24b]. Indeed, the utility of dynamic circuit operations in quantum computing more broadly has in fact already stimulated previous proposals of nonunitary parameterized quantum circuit architectures [CCL19; BF20; BM21; PBO20; IA24; YMZM24; Mel+24]. Our contribution in this work is to provide a unifying framework for dynamic PQC architectures, and to analyze both analytically and numerically their potential for variational quantum algorithms, with respect to the criteria discussed above.

1.1 Structure of this work

This work is structured as follows. We first give an overview of our contributions in Section 1.2. Next, in Section 2 we give a high-level overview of variational quantum algorithms, in order to provide both context and notation. Readers who are familiar with variational quantum algorithms could safely skip this section. We then proceed in Section 3 to introduce the dynamic parameterized circuit architectures we study here in more detail, and to discuss their relation to existing nonunitary parameterized

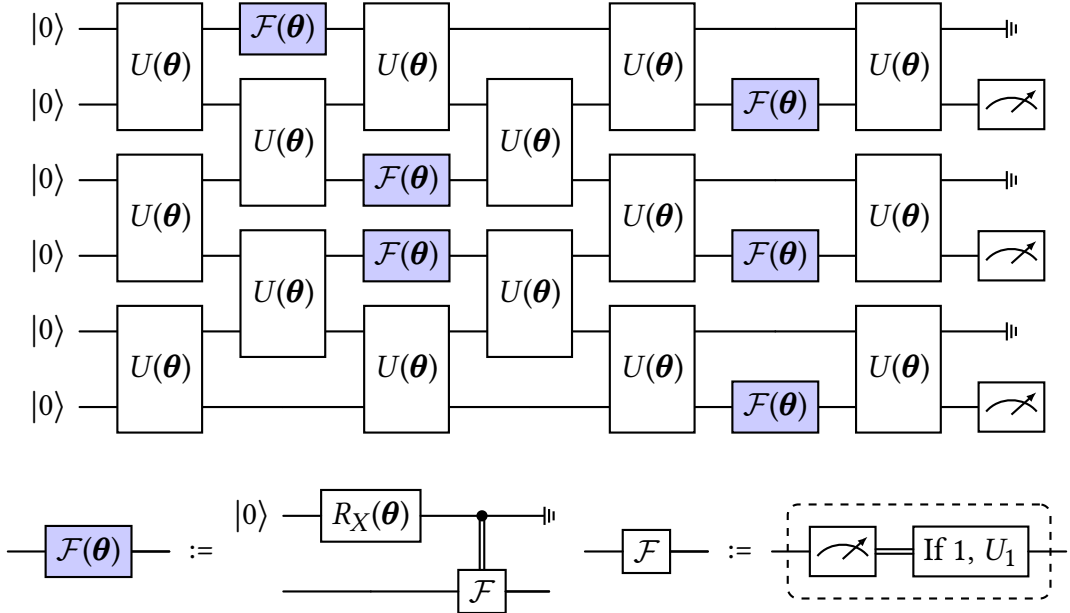


Figure 1: An illustration of the *dynamic* parameterized quantum circuit (DPQC) architectures that we consider in this work. These circuits consist of parameterized two-qubit unitary gates $U(\boldsymbol{\theta})$, as well as parameterized nonunitary single-qubit dynamic operations, which are denoted as $\mathcal{F}(\boldsymbol{\theta})$ -gates. Each such $\mathcal{F}(\boldsymbol{\theta})$ operation is a probabilistic implementation of a *feedforward* operation \mathcal{F} .

quantum circuit proposals. With this established, we study the trainability of DPQC architectures in Section 4. In particular, we begin with a discussion of what “trainability” actually means, and how this notion is related to barren plateaus. We then state our main analytical result, which provides sufficient conditions for the absence of barren plateaus in DPQC architectures. We then introduce the ingredients for the proof, namely a statistical mechanics model, and show how it can be used to derive existing barren plateau results. Given these theoretical foundations, we then provide the aforementioned numerical experiments for both ground and thermal state preparation in Section 5. Finally, we discuss in Section 6 the classical simulability of DPQC architectures.

1.2 Our results and contributions

1.2.1 Dynamic parameterized quantum circuits

First, we describe the dynamic parameterized quantum circuit (DPQC) architectures that we consider as variational ansätze in this work. They consist of layers of parameterized two-qubit gates $U(\boldsymbol{\theta})$ interspersed with parameterized dynamic operations $\mathcal{F}(\boldsymbol{\theta})$ (see also Fig. 1). We will denote the full parameterized dynamic circuit as a channel $\mathcal{C}(\boldsymbol{\theta})$ with parameters $\boldsymbol{\theta}$. While dynamic operations can in principle be applied across many qubits, in this work, we choose to focus on single-qubit dynamic operations. More specifically, as illustrated in Fig. 1, here each parameterized dynamic operation $\mathcal{F}(\boldsymbol{\theta})$ is a probabilistic implementation of a *feedforward* operation \mathcal{F} with probability $\sin^2(\theta/2)$. The feedforward operations themselves consist of a measurement on the respective qubit followed by a conditional gate: if the measurement outcome was 0, then apply $U_0 = I$, if instead it was 1, apply U_1 given by

$$U_1 = \begin{pmatrix} \cos \varphi e^{-i\phi} & -i \sin \varphi \\ -i \sin \varphi & \cos \varphi e^{i\phi} \end{pmatrix}. \quad (1)$$

We note that the ancilla qubits that control the probability of implementing \mathcal{F} operations are unentangled with the rest of the circuit, and can be simulated classically—i.e. one does not need an additional physical qubit for each $\mathcal{F}(\boldsymbol{\theta})$ operation. At the end of the circuit, an observable supported on some subset of the qubits is measured, in order to calculate the value of some loss function. We call the qubits on which this observable is supported *system* qubits, and refer to the remaining qubits as *ancilla* qubits.

We stress that the position of the dynamic operations in the circuit, the nature of the parameterized and conditional operations within the dynamic operations, and the number and allocation of system and ancilla qubits, are all design choices that one can make freely. Finally, given a parameterized dynamic quantum circuit $\mathcal{C}(\boldsymbol{\theta})$, at initialization we draw the parameters of the two-qubit gates $U(\boldsymbol{\theta})$ from a locally scrambling ensemble, which refers to an ensemble that is invariant under conjugation via single-qubit unitaries drawn from a unitary 2-design.

1.2.2 Expressivity

Having defined the parameterized dynamic circuit architectures that we study in this work, we start with two simple observations concerning the expressivity of these architectures.

Observation 1 (Expressivity of DPQC architectures with probabilistic feedforward—informal). Note that $\mathcal{F}(\theta = 0)$ is the identity channel. Therefore, by setting all the circuit parameters that control the probability of implementing an \mathcal{F} gate to 0, one obtains a purely unitary ansatz. With this in mind, given a DPQC architecture $\mathcal{C}(\boldsymbol{\theta})$ with connectivity graph G , let d be the depth of the architecture with all feedforward operations removed. This architecture can realize *all* unitary operations of depth d on G .

Said another way, if one starts from a unitary parameterized quantum circuit and then adds parameterized feedforward operations, the resulting DPQC architecture is at least as expressive as the unitary architecture from which one started. This observation is helpful, as it ensures us that one can in principle prepare interesting pure states using such an architecture. In the observation below, we highlight that even DPQC architectures with only *deterministic* feedforward operations (i.e. $\mathcal{F}(\theta) = \mathcal{F}(\pi)$) can realize nontrivial pure states.

Observation 2 (Expressivity of DPQC architectures with deterministic feedforward—informal). Consider any depth d DPQC architecture $\mathcal{C}(\boldsymbol{\theta})$, in which all feedforward operations are deterministic (i.e. happen with probability 1) and only occur on ancilla qubits (qubits on which the loss function has no support). Denote the connectivity subgraph of the system qubits in $\mathcal{C}(\boldsymbol{\theta})$ as G . Then, for every unitary circuit $U_{(d,G)}$ on G of depth d , there exists a setting of the parameters $\boldsymbol{\theta}$ such that $U_{(d,G)}$ is implemented by $\mathcal{C}(\boldsymbol{\theta})$.

The proof of the above observation is straightforward: simply observe that one can “disconnect” all ancilla qubits on which a dynamic operation occurs by setting any parameterized gate between a system qubit and such a qubit to be non-entangling. One is then left precisely with a depth- d parameterized circuit with connectivity graph G . Said another way, if one starts from a unitary parameterized quantum circuit of a certain depth and connectivity, and then adds ancilla qubits and feedforward operations on these ancilla qubits, the resulting parameterized dynamic quantum circuit is at least as expressive as the original unitary parameterized quantum circuit. We use parameterized dynamic circuit architectures with precisely such a structure for our ground state preparation experiments (See Section 1.2.4 and Section 5). In these experiments, we indeed observe convergence of our model to pure states. While we have not investigated whether this is the mechanism through which the model reaches pure states, the observation above again guarantees us that this is at least possible in principle.

1.2.3 Absence of barren plateaus

One of the primary contributions of this work is to provide sufficient conditions for the absence of barren plateaus in parameterized dynamic quantum circuit architectures. In purely unitary random circuits, the onset of barren plateaus is closely linked to the size of the observable’s *backward lightcone* [LWZ24; Lar+24]. Specifically, the loss function’s variance decays exponentially with the lightcone’s size due to the scrambling effect of the random unitary layers, which make the observable increasingly insensitive to individual parameter changes. We show that inserting feedforward operations \mathcal{F} fundamentally alters this behavior: each feedforward operation counteracts the scrambling, provid-

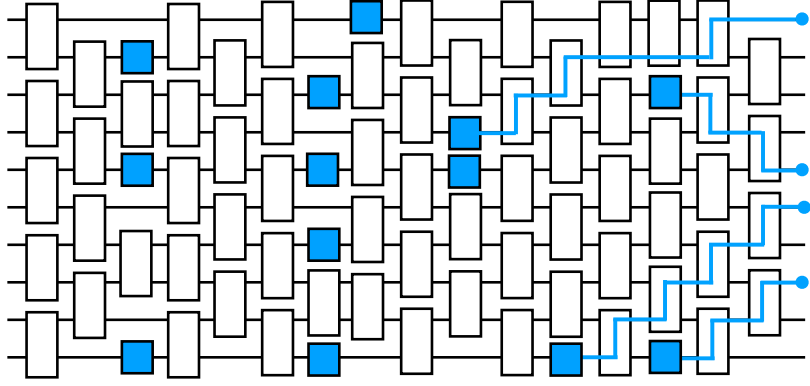


Figure 2: An illustration of the shortest paths from a qubit measurement to a feedforward operation through the backwards light cone of the measurement. The *feedforward distance* of an observable, with respect to a specific DPQC architecture, is the maximum length of such paths, over all qubits on which the observable is supported. Theorem 1 provides an upper bound on the variance of a local observable in terms of the feedforward distance.

ing a mechanism to prevent barren plateaus, without necessarily sacrificing expressivity. To quantify this, we introduce the *feedforward distance* f , which measures an observable’s distance to the nearest feedforward operation \mathcal{F} within its backward lightcone (see Figure 2 for a schematic explanation). We show a lower bound on the variance of the cost function that decays exponentially with feedforward distance f , rather than the size of the backward light cone.

Theorem 1 (Absence of barren plateaus in DPQCs for k -local Hamiltonians—informal). Let $\rho(\boldsymbol{\theta}) = \mathcal{C}(\boldsymbol{\theta})(|0^n\rangle\langle 0^n|)$ be the output state of the parameterized circuit ensemble introduced above and let H be a k -local Hamiltonian. Then, the variance of the loss function $L = \text{Tr } \rho(\boldsymbol{\theta})H$ is lower bounded as

$$\text{Var}_{\boldsymbol{\theta}} L \geq \left(\frac{\alpha}{5}\right)^{k(f+1)} \cdot \|H\|_{HS}^2, \quad (2)$$

where $\|H\|_{HS} := \sqrt{\frac{\text{Tr } H^2}{2^n}}$ is the normalized Hilbert-Schmidt norm of H and α is a constant that depends on the entangling power of the ensemble of two-qubit gates¹.

We note that for $k, f = O(1)$, the variance is non-vanishing. That is, we prove absence of barren plateaus for local observables under the condition that the feedforward distance f is constant. We emphasize that using this result, together with Observations 1 and 2, one can construct DPQC architectures which are both highly expressive and barren plateau free.

Additionally, we also show that the absence of barren plateaus in DPQC architectures is robust to noise present after every gate. Specifically, we show that when there is a unital single-qubit noise channel after every operation in the circuit with an average infidelity of $\gamma/2$, a similar lower bound on the variance holds.

Theorem 2 (Noise robustness of Theorem 1—informal). Let the output state of the noisy circuit be $\tilde{\rho}(\boldsymbol{\theta}) = \tilde{\mathcal{C}}(\boldsymbol{\theta})(|0^n\rangle\langle 0^n|)$. The variance of the loss function $L = \text{Tr } \tilde{\rho}(\boldsymbol{\theta})H$ for a k -local Hamiltonian is given by

$$\text{Var}_{\boldsymbol{\theta}} L \geq \left(\frac{\alpha(1-\gamma)^2}{5}\right)^{k(f+1)} \cdot \|H\|_{HS}^2. \quad (3)$$

Again, for $k, f = O(1)$ and $\gamma < 1 - \Omega(1)$, there is a nonvanishing variance of the loss function. This illustrates that the nonunitary feedforward operations help fight against noise-induced barren plateaus [Wan+21].

¹For Haar-random two-qubit gates, we have $\alpha = 1$.

On the technical side, Theorems 1 and 2 are proven via the so called “stat-mech” model [Hun19; DHB20; DHB21; Nap22; War+23], which allows one to compute second moments of statistical quantities of ensembles of random quantum circuits. In addition to using the stat-mech model to prove the above theorems, we also show how a variety of previous barren plateau results can be obtained via the stat-mech model, which may be of independent interest.

We stress that while a barren plateau result for a specific architecture indicates a significant obstacle to trainability [Lar+24], the absence of a barren plateau result does *not* immediately imply that an architecture is trainable in a meaningful sense [GGPD24]. We discuss this issue at length in Section 4.

Finally, we summarize the above insights into both expressivity and absence of barren plateaus with the following observation.

Observation 3 (DPQC architectures: connecting expressivity and absence of BPs). Taking together Theorem 1 on absence of BPs, and Observations 1 and 2 on expressivity, we note that DPQC architectures allow one to interpolate smoothly between highly expressive unitary architectures and BP-free nonunitary architectures with a constant feedforward depth.

1.2.4 Numerical results

In order to explore the potential utility of DPQC architectures for practically relevant problems, we perform numerical experiments for both ground and thermal state preparation problems.

Ground state preparation: For ground state preparation we study the perturbed toric code

$$H_{\text{toric}} = (1 - h)H_0 - \sum_{j=1}^n hZ_j \quad (4)$$

with open boundary conditions, as studied in [ZLZ24]. The first term of the Hamiltonian corresponds to the unperturbed toric code $H_0 = -\sum_v A_v - \sum_p B_p$, where v and p runs over all vertices and plaquettes of a 2D square lattice, and A_v and B_p represent the standard vertex and plaquette operators of the toric code. As discussed in [ZLZ24], this system is of interest as a test case as the ground state contains long-range entanglement. In Section 5.1 we provide the results of our experiments, for a square lattice of 12 system qubits and 4 ancilla qubits for different values of the perturbation h . In particular, we find that parameterized dynamic quantum circuits perform competitively with state-of-the-art variational parameterized quantum circuit architectures, such as those based on finite local-depth parameterized quantum circuits [ZLZ24]. We also highlight that, despite what one might expect, for these numerical experiments we find that optimization over DPQC architectures leads to circuit instances which prepare *pure states*.

Thermal state preparation: We study both the transverse field Ising model

$$H_{\text{TFI}} = -\sum_{j=1}^n X_j X_{j+1} - \frac{1}{2} \sum_{j=1}^n Z_j, \quad (5)$$

and an XY model

$$H_{\text{XY}} = -\sum_{j=1}^n \left[\frac{3}{4} X_j X_{j+1} + \frac{1}{4} Y_j Y_{j+1} \right] - \frac{1}{2} \sum_{j=1}^n Z_j, \quad (6)$$

with periodic boundary conditions, as has been studied in prior work on thermal state preparation with dissipative variational quantum algorithms [IA24]. In Section 5.2, we show the results of numerical experiments aimed at preparing the thermal states of the above models at inverse temperature $\beta = 2$, for a variety of circuit depths, and system sizes of up to 10 qubits. While these results provide evidence that DPQC architectures can indeed provide good approximations to the thermal states of interesting

models, we wish to highlight that they were obtained by using the infidelity with respect to the target thermal state as a loss function, which is *not* a scalable approach and is not covered by our results on the absence of BPs. As such, the results obtained provide evidence that DPQC architectures are capable of representing good approximations to the thermal states of interesting systems, but more work is required to understand the performance of such architectures with respect to other loss functions that can be measured efficiently on a quantum computer.

Finally, we note that for both the ground and thermal state preparation experiments above, the gradients were obtained by automatic-differentiation [Zha+23] executed via classical simulation. However, by considering the purification of the feedforward operations, one could also obtain a gradient estimator via a parameter shift rule which may be evaluated on a quantum computer, under some assumptions on the parameterized gates [WIWL22]. Further details are provided in Sec. 4.6.

1.2.5 Classical simulability

Lastly, in order to understand the potential utility of any variational quantum algorithm, it is crucial to understand the extent to which this variational quantum algorithm can or cannot be efficiently classically simulated, when used to solve relevant problems. For the DPQC architectures studied in this work, we find the following:

Worst-case hardness: It follows as an immediate consequence of Observations 1 and 2 that there are DPQC architectures which are both barren-plateau-free and worst-case hard to simulate classically. In particular, one can consider starting from any universal unitary circuit architecture, and then either introducing probabilistic feedforward operations, or deterministic feedforward operations on ancilla qubits, in such a way that the resulting DPQC architecture has constant feedforward depth. We stress that there are a variety of other strategies one could use for avoiding BP's, such as deep circuits with fixed or small-angle initializations, that would also lead to architectures which are BP-free and worst-case hard to simulate. However, intuitively, one expects randomness in initialization to be useful for optimization, and therefore for these alternative strategies to be disadvantageous from an optimization perspective.

Average-case easiness: For a wide class of DPQC circuit architectures $\mathcal{C}(\boldsymbol{\theta})$, with high probability over the choice of $\boldsymbol{\theta}$ at initialization, the circuit $\mathcal{C}(\boldsymbol{\theta})$ can be efficiently classically simulated—in the sense that expectation values of Pauli observables can be efficiently classically estimated—via low-weight Pauli path propagation [Ang+24].

Average-case easiness does not rule out quantum utility: Despite being average-case easy to simulate, DPQC architectures could still provide quantum utility if worst-case hard instances occur during training. Whether or not this is the case for DPQC architectures, when used to solve practically relevant problems, remains an open and interesting direction for future research.

We discuss all of these issues at length in Section 6.

2 Variational quantum algorithms

We begin with a brief overview of *variational quantum algorithms* (VQAs), in order to both set notation and provide a unifying framework for the results of this work. Readers familiar with variational quantum algorithms could skip this section and return to it when they encounter any notation which is defined here. The starting point for any variational quantum algorithm is a problem, defined by a loss function $L : \mathcal{X} \rightarrow \mathbb{R}$, for some set of objects \mathcal{X} . The solution to the problem L is given by

$$x^* = \arg \min_{x \in \mathcal{X}} L(x). \quad (7)$$

Some concrete examples of problems we might be interested in are:

Algorithm 1 Variational quantum algorithm

Given: Loss function $L : \mathcal{X} \rightarrow \mathbb{R}$
Choose: PQC architecture $\mathcal{C} = \{\mathcal{C}(\boldsymbol{\theta}) \mid \boldsymbol{\theta} \in \Theta\}$
Choose: Circuit-to-object map $M : \mathcal{C} \rightarrow \mathcal{X}$
Choose: initialization strategy IS

Choose: parameter update rule PU

Choose: convergence criteria CC

Define $L_M : \Theta \rightarrow \mathbb{R}$ via $L_M(\boldsymbol{\theta}) = L(M(\mathcal{C}(\boldsymbol{\theta})))$

Use initialization strategy IS to set initial $\boldsymbol{\theta}_0 \in \Theta$

▷ Initialize parameters via IS

converged \leftarrow false

 $i \leftarrow 0$
while not converged **do**

Run circuit $\mathcal{C}(\boldsymbol{\theta}_i)$ (possibly multiple times) to evaluate $L_M(\boldsymbol{\theta}_i)$ ▷ Evaluate loss function

if $L_M(\boldsymbol{\theta}_i)$ converged **then** ▷ Evaluate convergence using CC

converged \leftarrow true

else if $L_M(\boldsymbol{\theta}_i)$ not converged **then**

Use parameter update rule PU to determine $\boldsymbol{\theta}_{i+1} \in \Theta$ ▷ Update circuit parameters

 $i \leftarrow i + 1$
end if
end while

Return $\boldsymbol{\theta}_i$

▷ Output hypothesis circuit parameters

1. Ground state search: Let \mathcal{S}_n represent the set of n -qubit quantum states. The ground state search problem for an n -qubit Hamiltonian H is defined by the loss function $L_H : \mathcal{S}_n \rightarrow \mathbb{R}$, where $L_H(\rho) = \text{Tr}(\rho H)$. The solution to the problem is given by the ground state of the Hamiltonian.
2. Thermal state preparation: For a given Hamiltonian H and inverse temperature β , we aim to prepare the state that minimizes the free energy, i.e. the problem is defined by the loss function $L_{(H,\beta)} : \mathcal{S}_n \rightarrow \mathbb{R}$ where $L_{(H,\beta)}(\rho) = \text{Tr}[\rho H] + \frac{1}{\beta} \text{Tr}[\rho \log \rho]$. The solution to the problem is the Gibbs state $\rho_{\text{Gibbs}} = \frac{e^{-\beta H}}{\text{Tr}[e^{-\beta H}]}$.
3. Distribution learning: Let \mathcal{D}_n represent the set of all discrete distributions over length- n bit strings. The distribution learning problem for a target distribution $\mathcal{D} \in \mathcal{D}_n$ is defined by the loss function $L_{\mathcal{D}} : \mathcal{D}_n \rightarrow \mathbb{R}$ where $L_{\mathcal{D}}(\mathcal{D}') = d(\mathcal{D}', \mathcal{D})$, where d is some metric on distributions. The solution to the problem is the target distribution \mathcal{D} .
4. Quantum process learning: Let \mathfrak{T}_n represent the set of all n -qubit quantum channels, and let d_{\diamond} be the distance induced by the diamond norm. The quantum process learning problem for a target channel $\mathcal{T} \in \mathfrak{T}_n$ is defined by the loss function $L_{\mathcal{T}} : \mathfrak{T}_n \rightarrow \mathbb{R}$ where $L_{\mathcal{T}}(\mathcal{T}', \mathcal{T}) = d_{\diamond}(\mathcal{T}, \mathcal{T}')$. The solution to the problem is the target channel \mathcal{T} .

A standard approach to solving such problems is to perform optimization with respect to L , over some parameterized subset of \mathcal{X} , which we will refer to as a model class. Variational quantum algorithms follow this approach, using a parameterized quantum circuit (PQC) to define the model class. In this work, we will define a parameterized quantum circuit to be a circuit consisting of parameterized quantum channels. We describe the set of circuits as $\mathcal{C} = \{\mathcal{C}(\boldsymbol{\theta}) \mid \boldsymbol{\theta} \in \Theta\}$, where Θ represents the set of all possible channel parameters, and $\mathcal{C}(\boldsymbol{\theta})$ represents the concrete circuit instance associated with param-

eters $\boldsymbol{\theta}$. We note that many existing works on variational quantum algorithms consider parameterized quantum circuits which consist only of parameterized unitary gates. Importantly though, as we will see in Section 3, in this work we do *not* make such a restriction.

To define an appropriate model class from a parameterized quantum circuit \mathcal{C} , we also require a “circuit-to-object” map $M : \mathcal{C} \rightarrow \mathcal{X}$, which maps from quantum circuits to the set of objects \mathcal{X} on which the loss function L is defined. For the example problems given above, natural choices for the map M would be:

1. Ground state search and thermal state preparation: $M : \mathcal{C} \rightarrow \mathcal{S}_n$ via $M(\mathcal{C}(\boldsymbol{\theta})) = \mathcal{C}(\boldsymbol{\theta})(|0^n\rangle\langle 0^n|)$, i.e., $M(\mathcal{C}(\boldsymbol{\theta}))$ is the output state of the quantum circuit on the fixed input state $|0^n\rangle\langle 0^n|$.
2. Distribution learning: $M : \mathcal{C} \rightarrow \mathcal{D}_n$ via $M(\mathcal{C}(\boldsymbol{\theta})) = \mathcal{D}_{\boldsymbol{\theta}}$, where for all $x \in \{0, 1\}^n$ one has $\mathcal{D}_{\boldsymbol{\theta}}(x) = \langle x | \mathcal{C}(\boldsymbol{\theta})(|0^n\rangle\langle 0^n|) | x \rangle$ —i.e., $M(\mathcal{C}(\boldsymbol{\theta}))$ is the Born distribution associated with the output state of the quantum circuit on the fixed input state $|0^n\rangle\langle 0^n|$.
3. Quantum process learning: $M : \mathcal{C} \rightarrow \mathfrak{T}_n$ via $M(\mathcal{C}(\boldsymbol{\theta})) = \mathcal{C}(\boldsymbol{\theta})$ —i.e., $M(\mathcal{C}(\boldsymbol{\theta}))$ is simply the channel associated with the circuit.

Taking the parameterized quantum circuit together with the map M we can then define the model class $\mathcal{M}_{(\mathcal{C}, M)} \subseteq \mathcal{X}$ via

$$\mathcal{M}_{(\mathcal{C}, M)} = \{M(\mathcal{C}(\boldsymbol{\theta})) \mid \boldsymbol{\theta} \in \Theta\}. \quad (8)$$

We would now like to find the optimal model $m^* \in \mathcal{M}_{(\mathcal{C}, M)}$ with respect to L . This is equivalent to identifying the optimal circuit parameters $\boldsymbol{\theta} \in \Theta$ with respect to the loss function $L_M : \Theta \rightarrow \mathbb{R}$ defined via $L_M(\boldsymbol{\theta}) = L(M(\mathcal{C}(\boldsymbol{\theta})))$. A natural way to do this is via Algorithm 1, which provides an abstract template for any variational quantum algorithm. We stress that Algorithm 1 can be instantiated with a wide variety of different parameterized quantum circuit architectures, circuit-to-object maps M , initialization strategies, parameter update rules and convergence strategies. With this in hand, we proceed to introduce the class of dynamic parameterized quantum circuit architectures that we study in this work.

3 Dynamic parameterized quantum circuit architectures

In this section, we describe our proposed architectures and discuss their relation to existing nonunitary architectures.

3.1 Dynamic quantum circuits

A *dynamic* quantum circuit is one with intermediate measurements followed by one or more future operations conditional on the intermediate measurement results. In principle, any intermediate measurement can always be deferred to the end of the circuit. However, the standard way to do so incurs a cost of extra ancilla lines, taking up quantum space, a precious resource on current devices. As we will discuss below, dynamic circuit operations are a valuable computational resource, and as such the ability to natively perform dynamic operations on an architecture without introducing ancilla qubits is extremely valuable in a practical setting where there are limitations on the space and time overhead that may be tolerated.

In the setting of noisy quantum computation, the ability to remove entropy through intermediate measurements is extremely valuable and is fundamentally what enables quantum error correction. As shown in [ABIN96], when there is not an ability to pump in fresh ancilla qubits, depolarizing noise cannot be error-corrected. Ben-Or, Gottesman, and Hassidim [BGH13] characterize classes of single-qubit noise that allow for quantum error-correction in the setting where intermediate measurements are not allowed.

Another classic setting where measurements and feedforward operations play an important role is that of measurement-based quantum computation [Bri+09]. In this model, we prepare a standard, fixed, entangled resource state, which is then measured qubit by qubit in a basis that depends on the desired computation to be performed as well as the past sequence of measurement results.

Lastly, we discuss the idea of using intermediate measurements to spread correlations faster than otherwise unitarily possible. The crucial idea is that classical communication of measurement results from one part of the system to another in most hardware architectures is much faster than the time needed to apply a gate and can be assumed to be almost free. As an example, an unbounded quantum fanout gate may be applied in constant two-qubit gate depth, thus creating correlations between arbitrarily far qubits in $O(1)$ time [Bäu+24b; BW24; Son+24; Bäu+24a; Cór+21]. This would not have been possible using only unitary operations, which would need $\Omega(\text{diam}(G))$ depth to create nonlocal correlations between two vertices of the architectural graph G separated by $\text{diam}(G)$. Recently, this topic has received heightened interest, specifically with the viewpoint of classifying long-range entangled states [PSC21; LLKH22; BKKK22; TVV23b; Li+23] in many-body physics and strategies to prepare classes of states using adaptivity [BFLN23; MSWC24; Smi+24; PSC24]. For experimental demonstrations, see [Cór+21; TVV22; TVV23a; Fos+23; Bäu+24b; BW24; Son+24; Bäu+24a].

3.2 Dynamic parameterized quantum circuit architecture proposals

We now present the class of parameterized dynamic circuits that we argue are a promising class of circuits to consider for variational quantum algorithms. We present the full class of parameterized dynamic circuits for which our proofs hold in Appendix A.

We work with quantum circuits composed of two-qubit gates over n qubits with a total depth d . The total number of gates is denoted m . In this work, we also consider circuits with nonunitary operations, which we describe through channels, denoted by calligraphic letters such as \mathcal{U}, \mathcal{C} . For unitary channels, $\mathcal{U}(\rho) := U\rho U^\dagger$.

We begin with the notion of an architecture.

Definition 1 (Architecture). A quantum computing architecture is defined by a family of graphs whose vertices represent qubits. Edges connect vertices whose representative qubits may participate in a two-qubit operation in a layer of the circuit.

Definition 2 (Dynamic operation). A dynamic operation is a quantum channel that may be implemented via a projective measurement followed by a future operation conditioned on the measurement result.

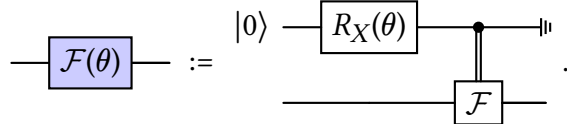
As an example, the simplest nontrivial dynamic operation is the following:

$$\text{---} \boxed{\mathcal{F}} \text{---} = \text{---} \boxed{\text{---}} \text{---} = \boxed{\text{---}} \text{---} \boxed{\text{If 1, } U_1} \text{---} . \quad (9)$$

Here, the state is measured, followed by a conditional gate U_1 if the measurement result is 1 and I otherwise. If we would like to perform a different operation U_0 when the result is a 0, we can account for it by adding a fixed gate after the feedforward operation as follows:

$$\text{---} \boxed{\text{---}} \text{---} = \boxed{\text{---}} \text{---} \boxed{\text{If 1, } U_0^\dagger U_1} \text{---} \boxed{U_0} \text{---} .$$

We can also simulate the probabilistic application of \mathcal{F} through a parameter θ that controls the probability with which it is applied, written out in purified form as:



The only role played by the parameter θ is to tune the state of the control qubit and hence the probability with which the target qubit is measured, given by $\sin^2(\theta/2)$.

In this work, we study the power of dynamic circuits with simple single-qubit feedforward operations \mathcal{F} . In our theoretical analysis, we study the case where $U_0 = I$ and U_1 is fixed to be

$$U_1 = \begin{pmatrix} \cos \varphi e^{-i\phi} & -i \sin \varphi \\ -i \sin \varphi & \cos \varphi e^{i\phi} \end{pmatrix}. \quad (10)$$

In some of our numerical results in Section 5, we also allow for these gates U_0 and U_1 to be parameterized.

Definition 3 (Parameterized dynamic circuit). A parameterized dynamic circuit \mathcal{C} of depth d on an architecture is a sequence of channels $\{\mathcal{U}_1(\boldsymbol{\theta}), \mathcal{U}_2(\boldsymbol{\theta}), \dots, \mathcal{U}_d(\boldsymbol{\theta})\}$, where each channel $\mathcal{U}_j(\boldsymbol{\theta})$ is a completely positive, trace preserving map on n qubits that describes the operations in time step j . The operations in each layer j can be written as a composition of single- and two-qubit operations such that the two-qubit operations act on non-overlapping qubits and only connect qubits with an edge in the associated graph describing the circuit architecture. The parameters $\boldsymbol{\theta}$ come from a set $\Theta \in \mathbb{R}^p$ for $p \in \text{poly}(n)$. The action of the entire circuit is described by the channel $\mathcal{C}(\boldsymbol{\theta}) = \mathcal{U}_d(\boldsymbol{\theta}) \circ \dots \circ \mathcal{U}_1(\boldsymbol{\theta})$.

Consider a loss function for which the circuit to object map defined earlier necessitates a circuit on n' output qubits. One way to define a parameterized dynamic circuit is as follows. Let $n = n' + n_a$ for a suitable integer n_a and let G be the architecture graph on n qubits describing the hardware connectivity. We consider edge colorings of the graph. An edge coloring is described by a list of colors $i = \{0, 1, 2, \dots\}$ together with the set of edges assigned the color i . The edge coloring defines a sequence of parameterized two-qubit unitary channels in the natural way: instantiate a parameterized two-qubit gate for every edge in a coloring and apply them in parallel. Then cycle through all the colors in the order $1, 2, \dots$ (we choose not to apply gates on the edges assigned the color 0). For a given graph, there can be several valid edge colorings, and each of these could potentially lead to a different ansatz. After every unitary layer $U_j(\boldsymbol{\theta})$, we apply the feedforward operation \mathcal{F} on a subset F_j of the n_a ancillary qubits. The j 'th channel of the parameterized dynamic circuit is given by $\mathcal{U}_j(\boldsymbol{\theta})(\cdot) = (\bigcirc_{i \in F_j}^n \mathcal{F}_i) \circ (U_j(\boldsymbol{\theta})(\cdot) U_j(\boldsymbol{\theta})^\dagger)$, where the symbol $\bigcirc_{i \in F_j}^n$ denotes a sequential composition of channels.

We illustrate in Fig. 3 a schematic dynamic circuit with feedforward operations. Here, the qubit lines 1, 3, and 5 are the ancillas that we trace over at the end of the circuit. The qubit lines 2, 4, and 6 are designated to be the system qubits on which the circuit-to-object map and the loss function are defined. The specific pattern of when and where we apply the feedforward operations $\mathcal{F}(\boldsymbol{\theta})$ is fixed beforehand during ansatz selection, along with the choice of an edge coloring and an order in which to apply gates in each block $U_1(\boldsymbol{\theta}), U_2(\boldsymbol{\theta}), \dots, U_d(\boldsymbol{\theta})$.

Lastly, we define a property of parameterized dynamic circuits, in terms of which we will state our main result on barren plateaus. This definition will use the notion of distance of an observable from a feedforward operation, which we describe more formally in Definition 14 (Appendix A). Informally, for a site j , the *feedforward distance* is the minimum number of entangling two-qubit gates that are encountered in the backwards light cone of qubit j before hitting a feedforward operation or the initial state. Figure 2 illustrates this definition.

Definition 4 (Informal version of Definition 14). A parameterized dynamic circuit is said to have a worst-case feedforward distance of f if, for every qubit j , the feedforward distance of j is at most f .

Our main result is on the sufficient conditions needed for a parameterized dynamic circuit to avoid barren plateaus.

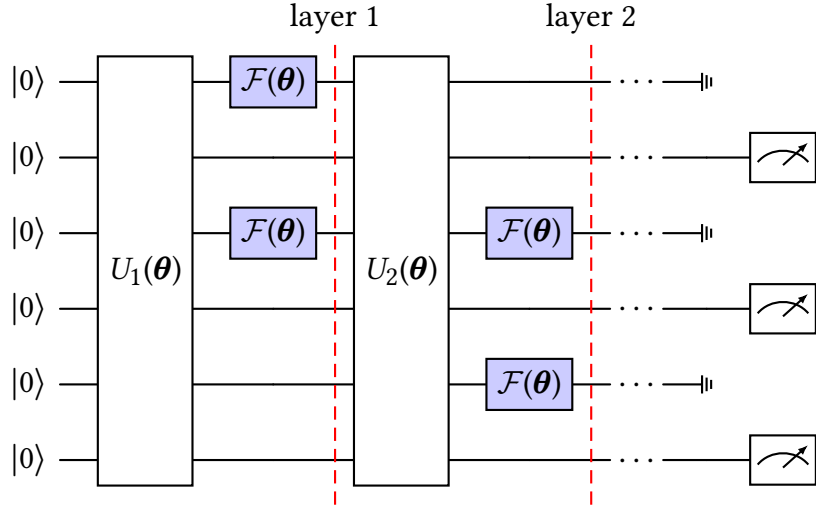


Figure 3: A schematic dynamic parameterized circuit on 6 qubits with 3 of them corresponding to ancillas.

3.3 Relation to existing nonunitary architectures

As mentioned in the introduction, there already exist in the literature a variety of proposals for nonunitary circuit architectures. Here we discuss the relation of our work to these existing proposals.

Perhaps the most prominent of existing nonunitary PQC architectures are Quantum Convolutional Neural Networks (QCNNs) [CCL19]. These are particularly interesting in light of their provable absence of barren plateaus [Pes+21]. QCNNs are designed around a very specific nonunitary operation, and as such can be seen as a particular subset of the PQC architectures that we study in this work. Indeed, one of our contributions is showing that nonunitary circuit operations can be used much more generally to avoid barren plateaus, without sacrificing circuit expressivity.

Another prominent class of nonunitary PQC architectures are the so-called dissipative quantum neural networks [Bee+20; BF20; BM21; PBO20]. The trainability of these architectures has also been studied to some extent [SCCC22], with both positive and negative results for specific architectural choices. Special cases of dissipative quantum neural networks coincide with special cases of dynamic PQC architectures we formulate and study here.

A related work is also that of [Mel+24], who study PQC architectures subject to *non-unital* noise. Indeed, one can view these non-unital noise channels as a specific instance of the nonunitary operations we allow for in DPQC architectures. However it is crucial to note that in the DPQC architectures we consider, one has control over the density, type and probability of nonunitary operations in the architecture, which is not the case for the PQC architectures with non-unital noise studied in [Mel+24]. As such, like we observed in Observation 3, the DPQC architectures we consider allow one to continuously interpolate between expressive unitary architectures and BP-free architectures, which is not the case for circuits subject to environmental non-unital noise. The extra control we allow for in our setup is a natural assumption to model current quantum hardware that has the capability of applying dynamic operations such as resets. As a consequence of the extra control, there is also a straightforward worst-case hardness result we can claim, even in the presence of noise, utilizing error-correction arguments.

Very recently, [IA24] and [YMZM24] introduced nonunitary PQC architectures involving mid-circuit measurements, similar to those we explore here. However, their focuses differ from ours. Specifically, [IA24] focuses on the noise resilience of these architectures, providing numerical evidence for their utility in thermal state preparation under noise but leaving the question of trainability and barren plateaus unresolved—issues we directly address here. Concurrently and independently, [YMZM24] explores state preparation using mid-circuit measurements to achieve shallow-depth circuits. To ensure

absence of barren plateaus, they require constant circuit depth. By contrast, our result on barren plateau absence (see Theorem 1) does not impose depth restrictions; rather, we characterize the absence of barren plateaus via the feedforward distance. Additionally, we apply a distinct technique, the statistical mechanics model, which may be of independent interest. Finally, we offer new insights into trainability beyond barren plateaus (c.f. Section 4) and classical simulability (c.f. Section 6) of these architectures.

4 Trainability

4.1 What does it mean for a PQC architecture to be trainable?

Having defined the dynamic parameterized quantum circuit (PQC) architectures we will study in this work, we now move on to a discussion of the “trainability” of such architectures within the context of variational quantum algorithms. Informally, and similarly to what is suggested in [GGPD24], we consider a PQC architecture \mathcal{C} to be *trainable* if with high probability Algorithm 1 converges, in a reasonable amount of time, to a set of circuit parameters $\boldsymbol{\theta}$ which is almost as good as the optimal circuit parameters

$$\boldsymbol{\theta}^* := \arg \min_{\boldsymbol{\theta} \in \Theta} L_M(\boldsymbol{\theta}). \quad (11)$$

Before trying to make the above notion more formal, there are a few points worth highlighting:

1. As the above notion of trainability relies on properties of Algorithm 1, it clearly depends not just on the PQC architecture \mathcal{C} , but also on the circuit-to-object map M , loss function L , parameter update rule PU, initialization strategy IS and convergence criteria CC. In particular, a PQC architecture \mathcal{C} may be trainable with respect to some set of these choices, and not trainable with respect to another set.
2. Importantly, the notion of trainability we have given above only requires that the circuit parameters $\boldsymbol{\theta}$ are almost as good as the best possible parameters in Θ . It *does not* put any additional “absolute” requirement on the optimal parameters. Said another way, it could be that even though $\boldsymbol{\theta}^*$ are the best possible parameters for our model class, the corresponding model $M(\mathcal{C}_{\boldsymbol{\theta}^*})$ is still a poor model. To get any stronger guarantee on the quality of the solution, we have to ensure that in addition to being trainable, \mathcal{C} also contains good solutions.

Essentially, we say that a PQC architecture \mathcal{C} is trainable, if we can efficiently and reliably find a set of circuit parameters defining a circuit which is almost as good, with respect to L , as the best solution we could hope to find within \mathcal{C} . With this in hand, a natural way to formalize the notion that a candidate set of parameters $\boldsymbol{\theta}$ is “almost as good”, would be if $L_M(\boldsymbol{\theta}) \leq L_M(\boldsymbol{\theta}^*) + \epsilon$ for some desired small ϵ . Additionally, we could say that Algorithm 1 converges “efficiently”, if it requires at most $\text{poly}(n, 1/\epsilon, 1/\delta)$ update steps, where n is the size of the problem, ϵ is the desired accuracy with respect to the optimal parameters, and δ is the desired probability of success².

Unfortunately, proving any formal trainability statement of the above type, for a nontrivial PQC architecture \mathcal{C} , realistic problem L and state-of-the-art parameter update rule PU, is formidably difficult [GGPD24]. However, while proving meaningful positive trainability results is difficult, it is often easier, at least for gradient-based parameter update rules, to prove *negative* trainability results via *barren plateaus* [Lar+24; Nie23]. At a high level, one says that a PQC architecture \mathcal{C} admits a barren plateau (BP) under initialization strategy IS if, with high probability when choosing the circuit parameters according to IS, one finds that the expectation value and variance of the gradient $\nabla L_M(\boldsymbol{\theta}_0)$ are exponentially close to zero. Intuitively, if this is the case then one expects the standard gradient descent parameter update rule $\boldsymbol{\theta}_{i+1} = \boldsymbol{\theta}_i - \alpha \nabla L_M(\boldsymbol{\theta}_i)$ to fail, as it can only lead to very small parameter changes

²We note that this definition of trainability looks extremely similar to the definition of agnostic learning [KSS92]. However, here L_M is the loss function which is actually evaluated and minimized during Algorithm 1—i.e., the *empirical* risk—whereas in the agnostic learning setting the requirement is with respect to the *true* risk.

in any polynomial number of update steps. We will discuss barren plateaus in much more detail in Section 4.2, however for our discussion here it is important to stress the following:

For a given PQC architecture \mathcal{C} , absence of a barren plateau is not sufficient for trainability.

More specifically, while the presence of a BP can be used to rule out trainability, the absence of a barren plateau does not prove trainability. To give an example, one could imagine a loss landscape filled with many local minima, none of which is ϵ -close to the global minimum with respect to L_M . In such a landscape, we would expect a gradient based update rule to efficiently find a local minimum, but this local minimum may not be good enough to satisfy the requirements of trainability.

Given all of the above, and in particular the difficulty of formally proving rigorous trainability statements for meaningful problems, we *do not* in this work prove trainability of dynamic parameterized quantum circuits. Instead, our approach in this work is to provide as much well motivated *evidence* for the trainability of dynamic parameterized quantum circuit architectures as possible. We do this by:

1. Proving an absence of barren plateaus for a natural distribution over circuit parameters—i.e. we show that this “necessary but not sufficient” condition for trainability is satisfied for dynamic parameterized circuit architectures that satisfy certain explicit criteria. This is done in Section 4.3.
2. Providing numerical experiments in Section 5 that show that, at least for one meaningful ground state search problem, gradient-based VQAs using dynamic parameterized quantum circuits can reach good solutions in a reasonable amount of time. We also leverage the nonunitary nature of DPQCs and additionally study problems where the target state is a mixed state, such as Gibbs states of certain Hamiltonians. Importantly, we also acknowledge and discuss caveats and criticisms of these numerical experiments in Section 5.3.

With this in hand, we proceed to provide a brief overview of barren plateaus, before proving our central absence of barren plateau result in Section 4.3.

4.2 Barren plateaus

Loss landscapes that are on average exponentially flat and gradients that are on average exponentially small in the number of system qubits—*barren plateaus*—represent a substantial bottleneck in the applicability of variational quantum algorithms to a practically relevant problem (size) [McC+18; Cer+21b; CC21; HSCC22; OKW21; Wan+21; Nap22; UB21]. In fact, they are one of the central challenges that might block the scalability of these algorithms. The causes for the occurrence of this phenomenon are multifold: ansatz depth or expressivity [McC+18; HSCC22], entanglement [OKW21], unital hardware noise [Wan+21], and loss functions induced by global observables, namely, observables acting on most system qubits [Cer+21b]. More specifically, a loss function $\mathcal{L}(\boldsymbol{\theta})$ is said to suffer from a barren plateau if, for all parameters $\boldsymbol{\theta}_k$, the variance of the gradient decays exponentially—i.e. $\text{Var}_{\boldsymbol{\theta}} [\partial_k \mathcal{L}] \in O(1/b^n)$ —with respect to $\boldsymbol{\theta}$ drawn from some natural distribution over Θ . As proven in [AHCC22], under some assumptions, this gradient behavior is often directly equivalent to an exponential concentration of the *loss function itself*, namely, $\text{Var} [\mathcal{L}] \in O(1/b^n)$ for some $b > 1$. Bounds on the concentration of both loss and gradients which may be computed efficiently with classical resources are given in [Nap22; LWZ24; UB21].

While strategies to circumvent barren plateaus are known, most of them suffer from drawbacks that limit their utility in practice. Firstly, one may use smart parameter initialization strategies [GWOB19; RMM+23; WQFD23; ZLHT22]. These, however only hold for the beginning of the training and do not help to exclude the occurrence of barren plateaus throughout the training. Moreover, parameter initialization according to distributions concentrated on small subsets of parameter space can restrict the ability to explore the space of good solutions. Another strategy to avoid exponentially flat loss landscapes is to choose ansatz classes which have been proven to not suffer from barren plateaus [Pes+21; SCCC22]. However, while being barren plateau free, the previously suggested ansatz classes suffer from restricted expressivity, e.g., due to a constant circuit depth or restricted dynamical lie algebra, which

in turn can easily lead to classical simulability of the respective model [Cer+23]. For a detailed review on barren plateaus, we refer the interested reader to [Lar+24].

4.3 Absence of barren plateaus in dynamic parameterized quantum circuits

We now state our first main result.

Theorem 3 (Variance bound for k -local Hamiltonians—formal version of Theorem 1). Let $\rho(\boldsymbol{\theta}) = \mathcal{C}(\boldsymbol{\theta})(|0^n\rangle\langle 0^n|)$ be the output state of the parameterized DPQC ensemble. In particular, assume that the ensemble $\mathcal{C}(\boldsymbol{\theta})$ satisfies the following properties:

1. Every component $\boldsymbol{\theta}_i \in \boldsymbol{\theta}$ parameterizes only a single operation in \mathcal{C} .
2. \mathcal{C} is locally scrambling, i.e., is invariant under single-qubit random gates from a unitary 2-design after every gate.
3. \mathcal{C} has constant worst-case feedforward distance f .
4. \mathcal{C} has an average entangling power of α [ZZF00; WSB03] and average swapping power $\beta \geq 0$ (see, for example, [War+23] for a definition of these parameters).

Let H be a k -local Hamiltonian and suppose it has an expansion $\sum_{\boldsymbol{\alpha}} c_{\boldsymbol{\alpha}} \boldsymbol{\alpha}$ in the Pauli basis $\boldsymbol{\alpha} \in \mathbb{P}_n$. Then, the variance of the loss function $L = \text{Tr } \rho(\boldsymbol{\theta})H$ with respect to the ensemble of circuits \mathcal{C} is lower bounded as

$$\text{Var}_{\boldsymbol{\theta}} L \geq \sum_{\boldsymbol{\alpha}} c_{\boldsymbol{\alpha}}^2 \left(\frac{\sin^2 \varphi}{3} \right)^{|\boldsymbol{\alpha}|} \left(\frac{\alpha}{5} \right)^{kf}. \quad (12)$$

For Hamiltonians whose terms are exactly k -local, this simplifies to

$$\text{Var}_{\boldsymbol{\theta}} L \geq \sum_{\boldsymbol{\alpha}} c_{\boldsymbol{\alpha}}^2 \left(\frac{\sin^2 \varphi}{3} \right)^k \left(\frac{\alpha}{5} \right)^{kf} = \|H\|_{HS}^2 \left(\frac{\sin^2 \varphi}{3} \right)^k \left(\frac{\alpha}{5} \right)^{kf}, \quad (13)$$

where $\|H\|_{HS} := \sqrt{\frac{\text{Tr } H^2}{2^n}}$ is the normalized Hilbert-Schmidt norm of H .

In the above, the invariance condition implies that the distribution over circuits is identical to the distribution where, after every operation, one inserts random single-qubit gate from any 2-design ensemble. The quantity α is related to the entangling power of the ensemble of 2-qubit gates [War+23]. We may also fix the 2-qubit gates deterministically.

Note the crucial point that these bounds are *independent* of the number of qubits n and the depth d of the circuit. This fact is what enables us to consider deep circuits of this form, restoring expressivity.

The proof idea of this result relies on the stat-mech model mapping described in the previous section. We extend these techniques to the case of more general nonunitary operations. The technique involves analyzing a biased random walk over a configuration space of identity and swap operators, interpreted as bitstrings $\{0, 1\}^n$. The walk is biased towards the 0 state. On the other hand, the variance of the loss function is related to the probability of obtaining a significant number of 1s, or large Hamming weight, in the output of the random walk.

In the presence of nonunitary operations, such as the simple measurement and feedforward operation mentioned above, we uncover a mechanism that changes the operator walk dynamics. Specifically, these operations add a new bias term in the reverse direction, causing a 0 to flip to a 1 with a certain nonzero probability. As we show in Lemmas 10 and 11, this mechanism is enough to lead to a lower bound on the probability of observing a nonzero Hamming weight at the output of the walk. This, in turn, yields a lower bound on the variance of the loss function.

4.4 The stat-mech model

We briefly review here the formalism of the statistical mechanical model (“the stat-mech model”) that allows us to compute second moments of statistical quantities over ensembles of random quantum circuits [Hun19; DHB20; DHB21; Nap22; War+23]. We review this more thoroughly in Appendix B. Concretely, the stat-mech model helps evaluate quantities of the form $\mathbb{E}_U[\text{Tr } \rho O]^2$ for an output state ρ of a quantum circuit with potentially nonunitary elements, averaged over the choice of random unitary gates U . This is done by observing that $\mathbb{E}_U[\text{Tr } \rho O]^2 = \mathbb{E}_U[\text{Tr } \rho^{\otimes 2} O^{\otimes 2}]$, which can be rewritten as $\text{Tr } \mathbb{E}_U[\rho^{\otimes 2}] O^{\otimes 2}$. This illustrates that the quantity $\mathbb{E}_U[\rho^{\otimes 2}]$, which we call the 2-copy average state, is the fundamental object of interest for calculating second moment quantities. Henceforth, we will denote this state by $\bar{\rho}$.

We can derive the stat-mech model by observing that the average two-copy state $\bar{\rho}$ can be classically tracked using the well-known Weingarten calculus for computing moments of the Haar measure. Specifically, if we assume that every 2-qubit gate or noise channel in the circuit is followed by a single-qubit Haar-random gate, then the state $\bar{\rho}$ lies in the symmetric subspace spanned by the operators $\{I, S\}^n$, where I is the identity operation and S the SWAP operation between the copies of the state. Using the trace-1 normalized versions of these operations $I := \frac{I}{4}$, and $S := \frac{S}{2}$, we can write

$$\bar{\rho} = \sum_{x \in \{0,1\}^n} c_x I^{1-x_1} \cdot S^{x_1} \otimes \dots \otimes I^{1-x_n} \cdot S^{x_n}, \quad (14)$$

where $\sum_x c_x = 1$. We thus see that the average two-copy state is characterized by a (quasi)-probability distribution over the space $\{I, S\}^n$. We will henceforth speak about the average two-copy state and its associated distribution \mathcal{D} over $\{I, S\}^n$ interchangeably. We also denote by \vec{x}^i the random variable corresponding to the string in $\{I, S\}^n$ at time i and by $\bar{\rho}_i$ the average two-copy state at time i .

In order to motivate the study of the stat-mech mapping in the context of barren plateaus in variational quantum algorithms, we state here a key lemma due to Napp [Nap22] relating the variance of the loss function to a quantity related to the average two-copy state. In Lemma 5 (Appendix B), we derive a generalization of Napp’s lemma to a more general setting where the two-qubit gates need not be chosen from a 2-design.

Lemma 4 ([Nap22]). The variance of a k -local observable h_i supported on a region A over an ensemble of quantum circuits of depth m with random single- and two-qubit gates chosen from a 2-design is

$$\mathbb{E}_V \mathbb{E}_{\theta} (\text{Tr } \rho(\theta) h_i)^2 = \Pr_{\mathcal{D}} \left[\prod_{i \in A} S^i \subseteq \vec{x}^m \right]. \quad (15)$$

In the above, the expectation over V is with respect to random (but unparameterized) gates V and that over θ is with respect to the parameterized gates of a specific form and \mathcal{D} the distribution over $\{I, S\}^n$ at the end of the circuit. We see, therefore, that the variance of the loss function directly depends on the distribution \mathcal{D} and whether it has high probability weight on strings $\in \{I, S\}^n$ that lead to the all S string on the subregion A .

4.5 A unified derivation of barren plateaus from the stat-mech model

In this subsection, we give a unified derivation of all known sources of barren plateaus in the stat-mech picture. This is done by examining the physical behavior of the stat-mech model on arbitrary geometries. This exercise will enable us to form intuition on the causes of barren plateaus, which will inform strategies to mitigate against them.

Let the reduced two-copy average state on two qubits at time i be $\bar{\rho}_i = aII + bIS + cSI + dSS$. Then the reduced two-copy average state after application of a unitary channel, given by $\bar{\rho}_{i+1} = \mathbb{E}_{V_1, V_2} [(V_1 V_2 \otimes$

$V_1 V_2) \mathcal{U} \otimes \mathcal{U}(\bar{\rho}_i)(V_1 V_2 \otimes V_1 V_2)^\dagger]$, can be expressed as $a' \mathbf{II} + b' \mathbf{IS} + c' \mathbf{SI} + d' \mathbf{SS}$, where

$$\begin{pmatrix} a' \\ b' \\ c' \\ d' \end{pmatrix} = T \begin{pmatrix} a \\ b \\ c \\ d \end{pmatrix} \quad (16)$$

for a 4×4 stochastic matrix T . For a Haar-random two-qubit unitary, the transfer matrix is given by [War+23]

$$T_{\text{Haar}} = \begin{pmatrix} 1 & \frac{4}{5} & \frac{4}{5} & 0 \\ 0 & 0 & 0 & 0 \\ 0 & 0 & 0 & 0 \\ 0 & \frac{1}{5} & \frac{1}{5} & 1 \end{pmatrix}. \quad (17)$$

From these facts, we see that for deep, random circuits on a well-connected architecture, the fixed point of $\bar{\rho}$ is given by $\frac{2^n}{2^{n+1}} \mathbf{II} \dots \mathbf{I} + \frac{1}{2^{n+1}} \mathbf{SS} \dots \mathbf{S}$. This implies that the probability of seeing any substring $\mathbf{S} \dots \mathbf{S}$ is at most $\frac{1}{2^{n+1}}$, giving barren plateaus for Hermitian observables of any locality. This observation also applies to circuits with fixed entangling gates, as long as the architecture is well-connected and every operation is followed by random single-qubit unitaries from a 2-design.

We can also easily derive in this formalism the statement on barren plateaus for random circuits of any depth with a global observable. The key is that when the initial state is a product state across all n qubits, its two-copy average state, $\bar{\rho} = \left(\frac{2}{3} \mathbf{I} + \frac{1}{3} \mathbf{S}\right)^n$ only has an inverse-exponential mass $\frac{1}{3^n}$ on the string $\mathbf{S} \dots \mathbf{S}$. Also observe that even in the limit $d \rightarrow \infty$, the mass $\frac{1}{2^{n+1}}$ remains inverse-exponentially small. Informally speaking, the distribution over $\{\mathbf{I}, \mathbf{S}\}^n$ is highly constrained and does not allow for a significant probability mass on the $\mathbf{S} \dots \mathbf{S}$ string at any depth. See [Nap22] for a more complete proof.

We now turn our attention to circuits with noise, as studied by [Wan+21]. With unital noise, the stat-mech model has an additional update rule given by the transfer matrix

$$T_{\text{noise}} = \begin{pmatrix} 1 & \gamma \\ 0 & 1 - \gamma \end{pmatrix}, \quad (18)$$

as detailed in Appendix B. This means that any \mathbf{S} string has a probability γ to “decay” into an \mathbf{I} string, which is a fixed point. In this case, as analyzed in [DHB21; War+23], the distribution rapidly converges to the $\mathbf{II} \dots \mathbf{I}$ fixed point. The probability of seeing an \mathbf{SS} string on any subregion decays exponentially in the number of gates applied on that subregion, or the local depth of the circuit.

Finally, we also discuss entanglement-induced barren plateaus [OKW21]. For this, we note that the relevant quantity we consider, the probability mass on any $\mathbf{SS} \dots$ string, is exactly the expected purity of the reduced density matrix on those sites. It often turns out for Lipschitz-continuous functions that one can get extremely good concentration bounds for random circuits. From concentration bounds, one can show the average logarithm of the purity is very well approximated by the logarithm of the average purity. A small mass on a $\mathbf{SS} \dots$ string thus implies a large negative logarithm of the purity on average, which in turn is related to the average Rényi-2 entropy.

4.6 Gradient evaluation

In this section, we show that the partial derivative of the cost function with respect to parameterized angles, as in Definition 3, can be evaluated using the parameter-shift rule [MNKF18; Sch+19]. Recall that a feedforward operation, $\mathcal{F}(\boldsymbol{\theta})$ can be parameterized using a unitary operation $R_X(\boldsymbol{\theta})$ on an ancillary qubit, followed by an operation on a system qubit. Therefore, the overall cost function can be defined as a unitary circuit, followed by a measurement of a Hermitian observable.

Let H denote a Hermitian observable and let θ_j denote a parameter such that the unitary circuit $\mathcal{C}(\boldsymbol{\theta})$ can be expressed as $\mathcal{C}(\boldsymbol{\theta}) = V_R(\boldsymbol{\theta}) \circ \exp(-i(\theta_j/2)P) \circ V_L(\boldsymbol{\theta})$, where P is a Pauli operator, and $V_L(\boldsymbol{\theta})$ and $V_R(\boldsymbol{\theta})$ parameterized unitaries positioned on either side of $\exp(-i(\theta_j/2)P)$. Note that we denote all parameterized angles together using $\boldsymbol{\theta}$.

Given an input state σ , the loss function L becomes

$$L(\theta_j) = \text{Tr} \left(H V_R \exp \left(-i \frac{\theta_j}{2} P \right) V_L \sigma V_L^\dagger \exp \left(i \frac{\theta_j}{2} P \right) V_R^\dagger \right), \quad (19)$$

where we denoted L as a function of θ_j alone, though it depends on other parameters $\boldsymbol{\theta}$ as well.

Define $B(\theta_j) := \exp \left(-i \frac{\theta_j}{2} P \right)$, $\Xi := V_R^\dagger H V_R$ and $\zeta := B(\theta_j) V_L \rho V_L^\dagger B(\theta_j)^\dagger$. The partial derivative of L with respect to θ_j is given by

$$\partial_j L := \frac{\partial L}{\partial \theta_j} = -(i/2) [\text{Tr} ([P, \zeta] \Xi)] \quad (20)$$

$$= -(i/2) \left[-i \text{Tr} \left([B^\dagger(\pi/2) \zeta B(\pi/2) - B^\dagger(-\pi/2) \zeta B(-\pi/2)] \Xi \right) \right] \quad (21)$$

$$= \frac{1}{2} [L(\theta_j + \pi/2) - L(\theta_j - \pi/2)]. \quad (22)$$

Thus, the gradient with respect of θ_j can be estimated by evaluating the cost function at two parameter-shifted values. When feedforward operations are modeled by a classical random variable $q(\phi_j)$ instead of a unitary on an ancillary qubit, the partial derivative involves updating the distributions $q(\phi_j + \pi/2)$ and $q(\phi_j - \pi/2)$.

5 Potential utility

Here we give evidence that the parameterized circuit architectures we propose indeed contain good solutions to interesting problems *and* that they can find these solutions in practice. In other words, we provide evidence that at scale they may provide “quantum utility”. We focus on both ground state and thermal state preparation. The setting that is explored in the context of ground state preparation almost³ satisfies the assumptions of Theorem 3, with deterministically applied feedforward operations at fixed locations in the circuit. For the setting of thermal state preparation, on the other hand, our numerical experiments are not in a regime where we expect Theorem 3 to hold, because they are based on the minimization of the infidelity between the output and target state, relying on a so-called *global* cost function.

5.1 Ground state preparation

In the following we are investigating the ground state problem for a Hamiltonian with 12 qubits that corresponds to a perturbed toric code. More specifically, the Hamiltonian is given as

$$H_{\text{toric}} = (1 - h)H_0 - \sum_{j=1}^n hZ_j, \quad (23)$$

where the first term corresponds to the unperturbed toric code $H_0 = -\sum_v A_v - \sum_p B_p$, with v and p running over all vertices and plaquettes of the corresponding 2D square lattice and A_v and B_p representing

³The numerical experiments feature a slightly different ensemble over single-qubit gates. Specifically, in Fig. 4, we consider the U_3 gate to have the Euler form $U_3 = R_Y(\theta_1)R_Z(\theta_2)R_Y(\theta_3)$ with a uniform distribution over angles $\theta_{1,2,3} \sim \mathcal{U}[0, \pi]$. In order to have a single-qubit 2-design, the middle angle θ_2 should instead be chosen from a distribution such that $\cos \theta_2 \sim \mathcal{U}[0, 1]$.

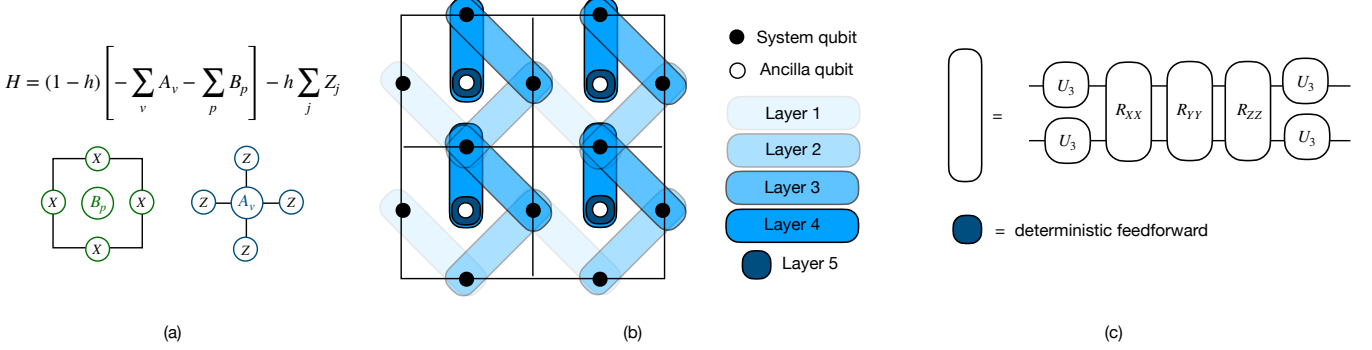


Figure 4: An illustration of the Hamiltonian and DPQC architecture used for ground state experiments. (a) The Hamiltonian is the perturbed toric code, for a system on a square lattice, with system qubits on the edges. (b) One layer of the ansatz consists of five sublayers. The first four are parameterized two-qubit unitary entangling gates, and the last sublayer consists of deterministic reset gates on all ancilla qubits. Gates are applied from lightest to darkest, so that all gates of the same opacity are applied in parallel. (c) Structure of the gates within each sublayer. U_3 denotes a generic single-qubit rotation gate with 3 Euler angles.

vertex and plaquette operators, respectively, which are given by products of X and Z Pauli operators. Notably, this model has also been investigated in [ZLZ24]. The ground state of this system exhibits long-range entanglement—a property that makes the representation, e.g., with tensor networks difficult. In order to entangle two qubits with a circuit that consists of single and two-qubit gates—as most hardware efficient ansätze—that are at distance n one needs, even if all-to-all connectivity is given, at least $\mathcal{O}(\log(n))$ two-qubit gates.

We build our ansatz layers as shown in Figure 4. In particular, each layer of the ansatz consists of five sublayers. the first three sublayers consist of parameterized unitary two-qubit entangling gates applied between system qubits, organized in such a way that in each sublayer all two-qubit gates are applied in parallel. The fourth sublayer consists of an entangling gate between the top qubit of each lattice block, and the ancilla in the centre of each lattice block. The structure of each two qubit gate is shown in Figure 4 (c). Finally, the fifth sublayer consists of deterministic resets applied to each ancilla qubit. In the presented experiments, we employed a total of two layers, of five sublayers each. At this point it should be noted that our ansatz is different from the ansatz employed in [ZLZ24] as all two-qubit gates in a sublayer are applied in parallel, hence reducing the ansatz depth. A deep version of this structure *without ancillary resets* was tested in the above mentioned reference but did not perform well. As illustrated in Fig. 5, we do not observe these performance issues which we conclude to be circumvented via the insertion of ancilla qubits which are regularly reset.

The initial parameters are drawn at random from a uniform distribution $[0, \pi)$. We use the ADAM optimizer [KB15] with a learning rate of 10^{-2} and at most 2000 iterations. The statistics for the different values of h are evaluated from 100 trial runs. The only exception of these settings are the experiments for $h = 1.0$, which had already converged after 500 steps and with 25 trials. All experiments were simulated with a tensor network simulator *TensorCircuit* [Zha+23], using a purification on 24 qubits for simplicity of code integration.

The examples shown in Fig. 5 illustrate that the training converges quickly for all trials and the different values of h . The larger h the faster the convergence in terms of energy and purity.

As illustrated in Fig. 6(a), the average best found energy matches the exact energy well for $h \geq 0.5$ with a standard deviation ≤ 0.022 . The best energies found per value for h matches the exact energy quite well with differences ≤ 0.078 for all tested values of h . Furthermore, it is particularly interesting to note that Fig. 6(b) illustrates how the states throughout the training are mostly mixed. However, when the state approaches the ground state energy the purity increases.

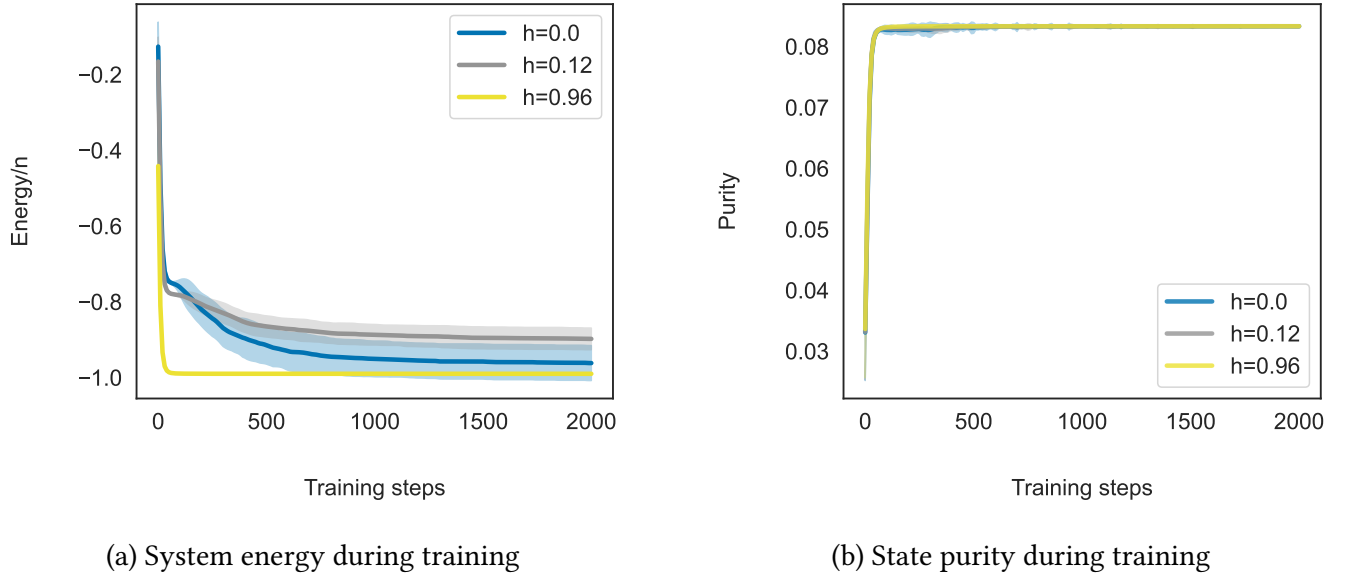


Figure 5: Variational training of a DPQC architecture for a perturbed toric code Hamiltonian acting on 12 qubits. The perturbation strength is controlled by the parameter h . All settings were run for 100 different seeds. The figure presents average and standard deviation of the respective outcomes. The convergence of training as a function of $h = 0, 0.12$ and 0.96 depicted in (a). The results indicates quick convergence for all trials and bigger h values converges faster. The purity value for the same h values has been shown in (b) indicating fast convergence with a good accuracy.

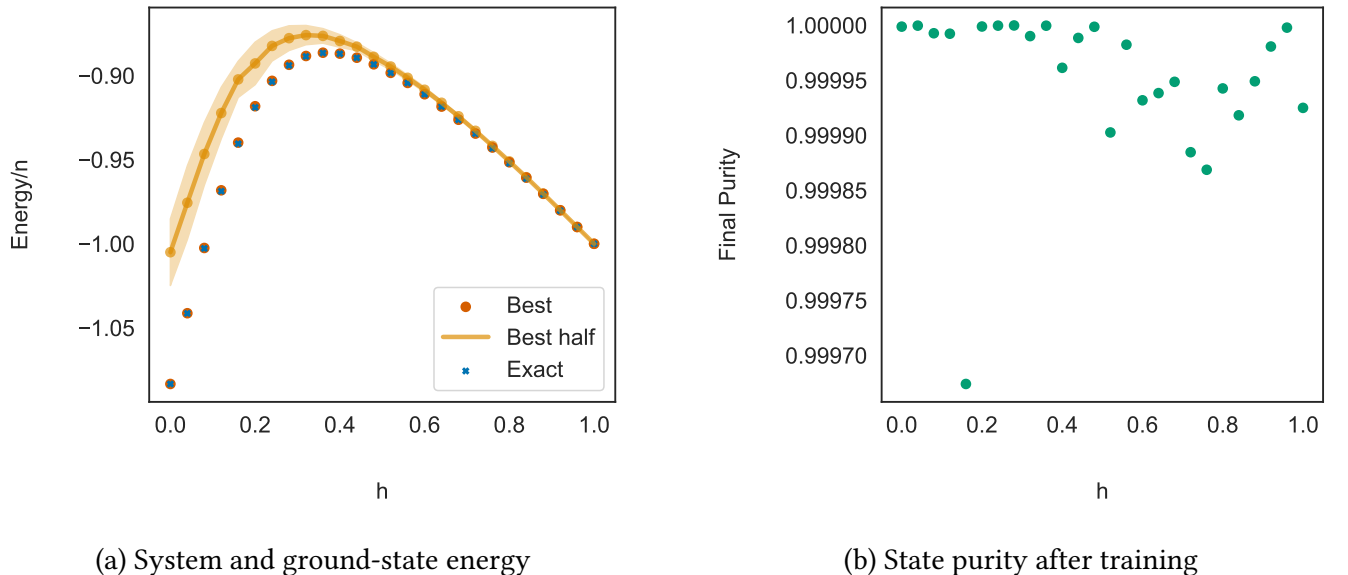


Figure 6: (a) The exact ground-state energy compared to that output by the variational algorithm, measured in terms of the best out of 100 trials (“best”) and the average over the best 50 out of 100 trials (“best half”); and (b) the purity of the final output state for different values of h , averaged over all 100 trials. For each h , the best estimate coincides with the exact ground-state energy.

5.2 Thermal state preparation

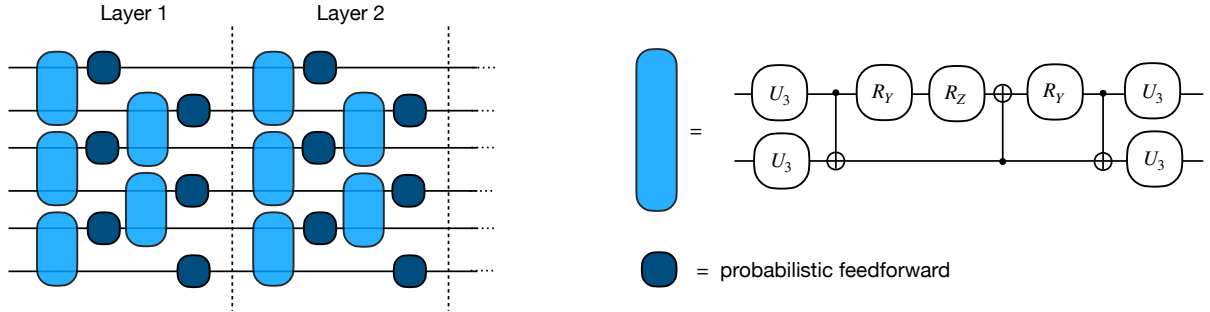


Figure 7: An illustration of the ansatz used for thermal state experiments, for a 6 qubit example. U_3 denotes a generic single-qubit rotation gate with 3 Euler angles.

Next, we investigate the applicability of our ansatz structure to thermal state preparation—which unlike ground state preparation typically leads to a mixed state. More specifically, we are looking to prepare a state of the form

$$\rho(H, \beta) = \frac{e^{-\beta H}}{\text{Tr}[e^{-\beta H}]}, \quad (24)$$

with β representing the inverse temperature. Notably, sampling from a thermal state at low temperature is known to be NP-hard [GSV16]. While it is possible to generate a mixed state in a unitary parameterized quantum circuit with auxiliary qubits, the DPQC architecture we work with is a natural fit for the task at hand.

We consider a transverse field Ising model

$$H_{\text{TFI}} = - \sum_{j=1}^n X_j X_{j+1} - \frac{1}{2} \sum_{j=1}^n Z_j, \quad (25)$$

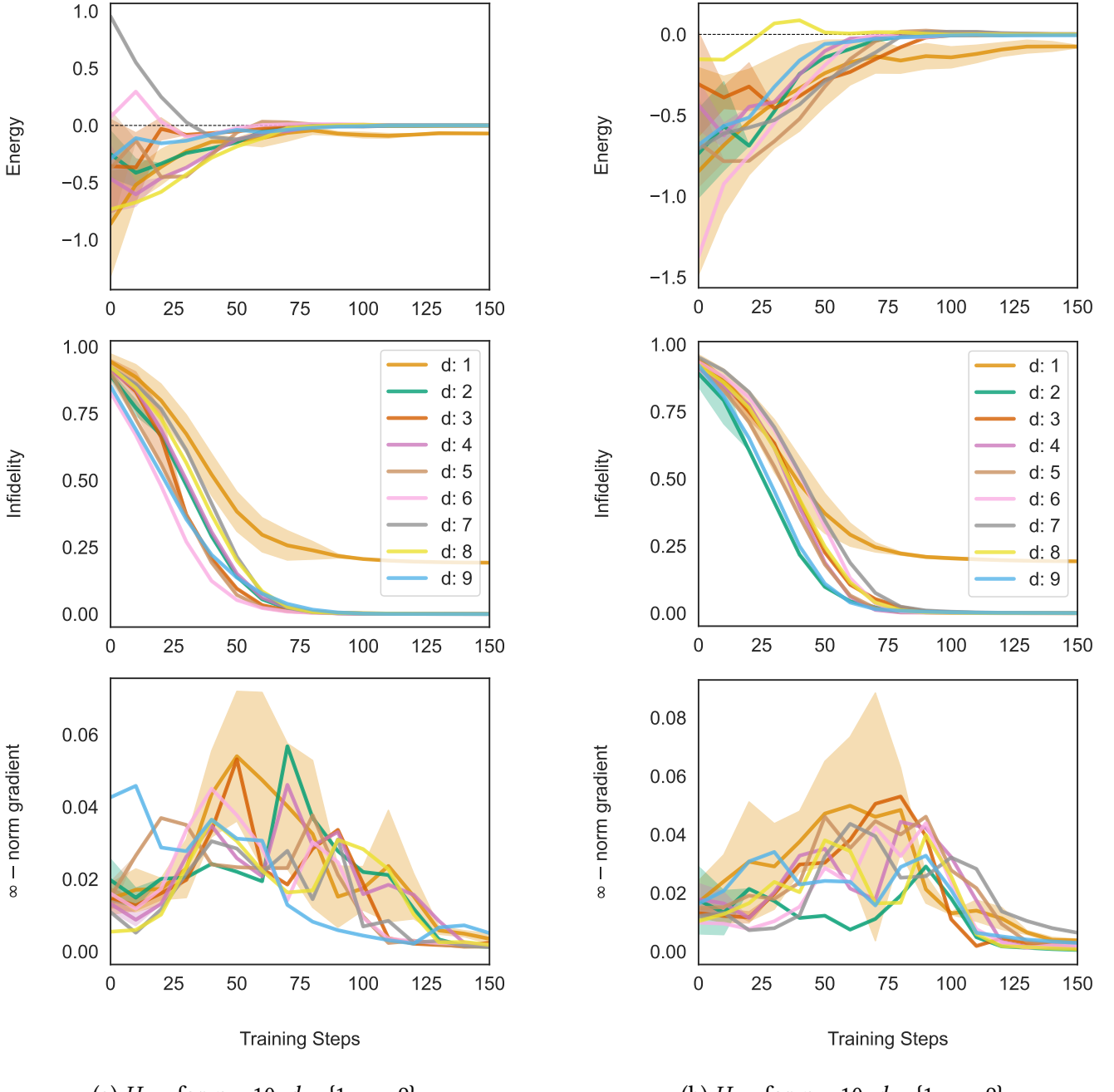
and an XY model

$$H_{\text{XY}} = - \sum_{j=1}^n \left[\frac{3}{4} X_j X_{j+1} + \frac{1}{4} Y_j Y_{j+1} \right] - \frac{1}{2} \sum_{j=1}^n Z_j, \quad (26)$$

both on a periodic 1D chain for up to 10 qubits. These systems were also investigated for up to 6 qubits in [IA24]. Notably, the dissipative ansatz suggested in [IA24] is compatible with the model discussed in this work—provided that the dissipative gates are set to be probabilistic feedforward operations $\mathcal{F}(\theta)$ where the application probability is controlled by a trainable parameter.

Notably, the action of $\mathcal{F}(\theta)$ corresponds to applying the identity operation with probability $p(\theta)$ and a reset on to the $|0\rangle$ state with probability $1 - p(\theta)$. The reset on to $|0\rangle$ can be implemented straightforwardly with a feedforward operation by setting in Eq. (9) the correction operation U_1 after measurement to be the X gate. An illustration of the ansatz structure is depicted in Fig. 7 for 6 qubits. More specifically, the figure illustrates the layers of the ansatz and their decomposition into sublayers. Notably, after the application of d layers as illustrated in Fig. 7, a final layer of unitary gates is applied, which is a special case of a $d + 1$ -layer DPQC up to the removal of the feedforward operations. The experiments shown in [IA24] demonstrate that this ansatz can prepare thermal states up to small errors with a number of layers equal to n . We study the induced training behavior for layer numbers $d = \{1, \dots, n - 1\}$ which helps us understand whether a shallower form of this ansatz class is already sufficiently expressive to approximate the thermal states with good accuracy.

We train the model $\tilde{\rho}(\theta)$ by minimizing the infidelity to the target state $\rho(H, \beta)$, i.e. $1 - F(\tilde{\rho}(\theta), \rho(H, \beta))$. While this type of cost function cannot be efficiently probed with small error on a quantum computer,



(a) H_{TFI} for $n = 10$, $d = \{1, \dots, 9\}$

(b) H_{XY} for $n = 10$, $d = \{1, \dots, 9\}$

Figure 8: The behavior of the energy, infidelity, and infinity norm of the gradient throughout 150 training iterations for the (a) transverse field Ising (b) XY model for various number of layers d . Notably, the target energy is indicated by a black horizontal line in the top plots.

it enables us to study the expressivity of our ansatz. We choose the initial parameters at random from a uniform distribution $[0, 1]$ and the target inverse temperature $\beta = 2$. Similar to the example on ground state preparation, we optimize with ADAM using a learning rate of 10^{-2} and simulate the systems with the density matrix integration of *TensorCircuit* [Zha+23]. All experiments were executed with 5 different randomly chosen seeds. The results presented in Fig. 8 show the average of those runs as well as the respective standard deviation thereof. The plots illustrate that in both cases the training already converges to infidelities of the order 10^{-5} with $d = 2$ layers and that the norm of the gradient magnitude for the model parameters does not decrease for larger d –despite the global form of the infidelity as a cost function. In fact, based on the observed convergence behavior and the magnitude of the loss function gradients, we are encouraged to test whether the ansatz can also work with more scalable loss functions for preparing thermal states [ZLW21; WLW21].

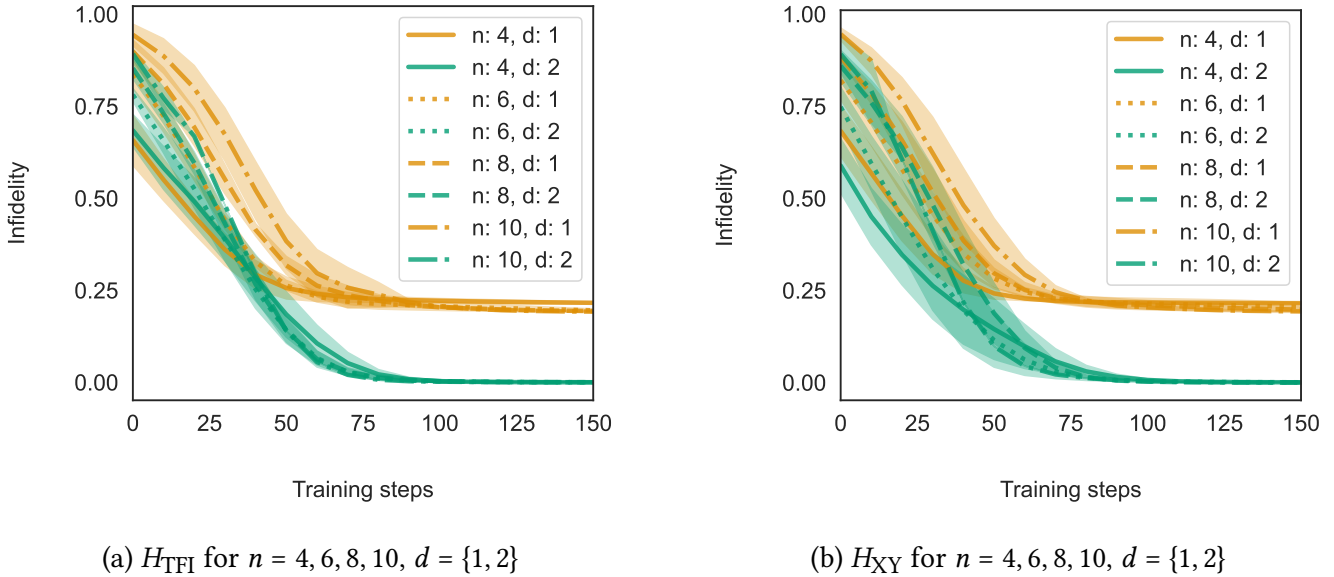


Figure 9: The behavior of the infidelity with respect to the target state throughout 150 training iterations for $d = 1$ and $d = 2$ for the (a) transverse field Ising (b) XY model.

A similar training behavior can be observed for 4, 6, and 8 qubits as shown in Fig. 9. More specifically, 2 layers seem to provide sufficient expressivity for training a good approximation of the target thermal state.

5.3 Caveats and criticisms

We note some caveats on these numerical experiments that may limit their applicability for other practical situations.

1. **Small-scale experiments:** We study relatively small system sizes, with a number of system qubits at most 12. In particular, this means that even an exponentially small gradient might not be very small.
2. **No shot noise:** It should be noted that since we used a tensor network simulator to simplify the evaluation of expectation values, the results are devoid of shot noise. Hence, we could in principle resolve exponentially small gradients faithfully should they occur throughout the training.
3. **No hardware noise:** Using numerical simulations with tensor networks means that the results are not affected by the noise typically present in actual quantum hardware. If we were to run our experiments on quantum hardware, we would expect the results to be influenced by this hardware-induced noise.
4. **Thermal state preparation is not scalable:** The thermal state preparation algorithm is based on a cost function that requires the evaluation of the fidelity. Given that one might require exponential measurement resources to estimate this quantity, the training pipeline is not scalable in its current form.

We note a few reasons to be optimistic about DPQCs despite these caveats. For example, note that [ZLZ24] studied the perturbed toric code model at the same system size. Even at these system sizes, they noted that linear-depth architectures for the preparation of the toric code state failed on account of barren plateaus. Furthermore, we note that as shown in Fig. 8, the norm of the gradient for the DPQC architecture is not very small in general, raising the possibility that it can be meaningfully estimated. There is also hope that in implementations of variational quantum algorithms, if hardware noise is consistent across runs, then its effect may be surmounted when implementing the algorithm [SKCC20]. Lastly, finding a suitable and scalable loss function for thermal state preparation with the

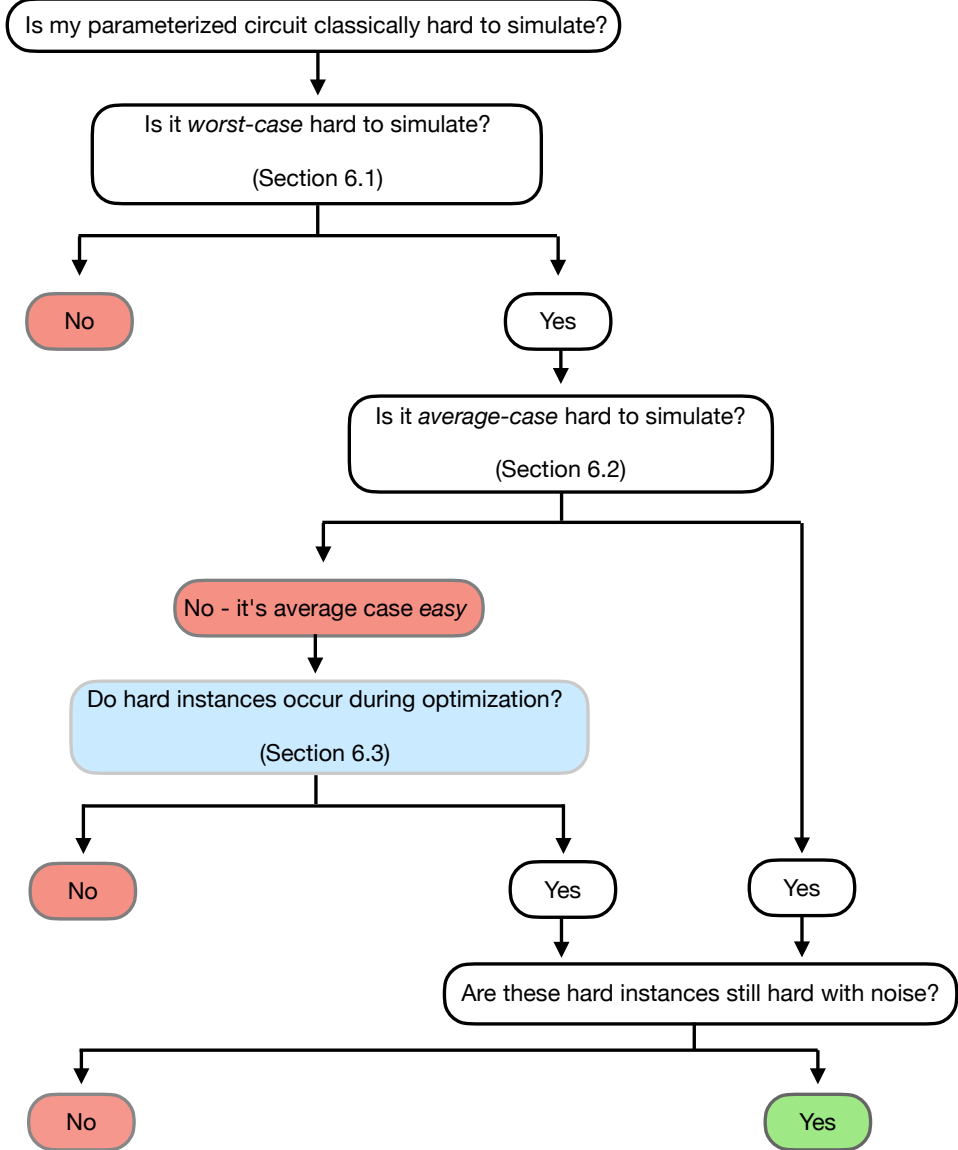


Figure 10: A methodology for determining whether a parameterized circuit class is classically hard to simulate. For the dynamic parameterized circuits considered in this work, we attempt to provide answers to the necessary questions in the sections indicated.

property that the optimum is close to the target Gibbs state is still an open problem. Testing some scalable cost functions [ZLW21; WLW21] could help make conclusive statements about the capabilities of our ansatz for thermal state preparation. Therefore, despite the caveats we point out, our results in this section may be viewed as promising first steps towards establishing the general utility of DPQC architectures in practical situations.

6 Classical hardness

In the section above, we have seen evidence that, at least for small problem sizes, variational quantum algorithms using dynamic parameterized quantum circuits can feasibly provide meaningful results for interesting problems. In this section we would finally like to address the question of whether these variational quantum algorithms, which use the dynamic parameterized quantum circuits we consider in this work, could be efficiently classically simulated when used to solve interesting and relevant large-scale problems. In particular, as we have already mentioned, in order for quantum devices to offer meaningful utility via these variational quantum algorithms, it is necessary that they *cannot* be efficiently classically simulated as problem and device sizes scale.

To begin, we refer back to the presentation of a variational quantum algorithm, presented in Section 2 as Algorithm 1. Specifically, we note that in order to classically simulate *a single iteration* of Algorithm 1, it is sufficient to be able to classically simulate:

1. The evaluation of the loss function $L_M(\boldsymbol{\theta}_i)$ for current circuit parameters $\boldsymbol{\theta}_i \in \Theta$.
2. The parameter update rule $\text{PU}(\boldsymbol{\theta}_i) = \boldsymbol{\theta}_{i+1}$.

In practice, for gradient based parameter update rules, it is sufficient to be able to evaluate the loss function L_M at $\boldsymbol{\theta}_i$ and small perturbations of $\boldsymbol{\theta}_i$ [WIWL22]. As such, we restrict our attention to classical simulation of the loss function $L_M : \Theta \rightarrow \mathbb{R}$ and assume that this is also sufficient for simulation of the parameter update rule. Additionally, by the design of variational quantum algorithms, evaluating the loss function L_M on a quantum device, at some $\boldsymbol{\theta} \in \Theta$, requires running the circuit $\mathcal{C}(\boldsymbol{\theta}) \in \mathcal{C}$, and then either collecting measurement results in the computational basis, or with respect to some local observable. In this work we will focus on the setting where the loss function can be calculated from the expectation value of local observables. As such in order to determine the extent to which the loss function can be classically simulated, it is sufficient to determine the extent to which, when given some local observable O and circuit parameters $\boldsymbol{\theta}$, one can obtain the expectation value of O , with respect to the output state of the circuit $\mathcal{C}(\boldsymbol{\theta})$. We refer to this problem as the problem of simulating a parameterized quantum circuit,

and as it implies the ability to simulate a single iteration of a variational quantum algorithm, it is the problem whose classical complexity we focus on in this section.

With this in mind, we proceed to analyze in the following sections the question of whether or not dynamic parameterized quantum circuits (DPQCs) can be efficiently classically simulated, by following the methodology illustrated in Figure 10. More specifically, we begin by first exploring in Section 6.1 whether or not DPQCs can be simulated in a *worst-case* sense. As per the decision tree in Figure 10, if the DPQC is *not* worst-case hard to simulate—i.e. if $\mathcal{C}(\boldsymbol{\theta})$ can be efficiently simulated for all $\boldsymbol{\theta} \in \Theta$ —then by the arguments discussed above this simulation algorithm can be used to simulate any variational quantum algorithm using the DPQC. However, in Section 6.1 we leverage the expressivity of DPQC’s to show that they are indeed worst-case hard to efficiently classically simulate, and that they therefore pass this first obstacle for classical simulations.

In light of this worst-case classical hardness, we then proceed to study the *average-case* hardness of classical simulations, with respect to circuit instances drawn from some natural distribution over Θ . Here we will show that, contrary to what one might hope, DPQCs are in fact *easy* to simulate on average, via the low weight Pauli-path algorithm recently studied in [Ang+24]. This average-case easiness of DPQCs then forces us to consider in Section 6.3 the subtle question of whether or not instances which are hard to simulate might occur during the execution of variational quantum algorithms using DPQCs, for interesting and relevant problems. In particular, here we argue that there could exist problems for which hard-instances for classical simulation might occur during the execution of a DPQC-based variational quantum algorithm, and we provide a precise open question whose answer could resolve this issue.

6.1 Worst-case hardness

In this section we observe that there exist DPQC architectures which are both barren plateau free, and worst-case hard to simulate classically (under standard complexity theoretic assumptions). To this end, consider a DPQC architecture constructed in either one of the following two ways:

1. Start with any universal unitary parameterized circuit architecture, and add *probabilistic* feed-forward operations in such a way that ensures the feedforward distance of the resulting DPQC architecture is constant.
2. Start with any universal unitary parameterized circuit architecture, and add *deterministic* feed-

forward operations on ancilla qubits, together with entangling operations between system and ancilla qubits, in such a way that ensures the feedforward distance of the resulting DPQC architecture is constant.

From Observations 1 and 2 both DPQC architectures above will be at least as expressive as the unitary architecture from which one started, and therefore worst-case hard to simulate classically unless $\mathbf{BPP} = \mathbf{BQP}$. Additionally, under some additional easy to satisfy assumptions on the parameterized gates, both architectures will also be barren plateau free via Theorem 1 and the assumed constant feedforward distance. Taken together we have:

There exist DPQC architectures that are both worst-case hard to classically simulate efficiently, and barren-plateau free!

From the above it is clear that the worst-case hardness is a simple consequence of the fact that one can design DPQC architectures which are expressive enough to contain universal unitary architectures. As such, we stress that one could straightforwardly make a similar statement about worst-case hardness and absence of BPs by simply considering universal unitary architectures with a fixed (or highly constrained) initialization strategy—eg, initializing to the identity. However, as optimization with such an initialization strategy would always start from the same region (or point) in the cost landscape, one would expect such a strategy to be disadvantageous from an optimization perspective. Ultimately, however, large-scale numerical experiments are necessary to distinguish the practical utility of these two approaches to balancing expressivity and trainability.

6.2 Average-case hardness (easiness)

As illustrated in Figure 10, in order to have any potential of providing utility via quantum devices, it is necessary but not sufficient for a parameterized quantum circuit architecture to be worst-case hard to classically simulate efficiently. Indeed, it could be the case that there exist hard circuit instances, but that these are never encountered during the execution of a variational quantum algorithm, which can therefore be efficiently classically simulated despite the worst-case hardness. Given this, having passed the first obstacle of worst-case classical simulation, we study in this section the *average-case* hardness of classically simulating the DPQC architectures relevant to this work.

Unfortunately, contrary to what one might hope, a large class of DQPC architectures—including the ones we use for numerical experiments in Section 5—are in fact average-case *easy* to efficiently classically simulate, via the low weight Pauli-path algorithm recently studied in [GD18; Aha+22; SWCL23; Fon+23; SYGY24; Ang+24]. More specifically, we can make the following observation:

Observation 4 (Average-case easiness of DPQC simulation via low-weight Pauli paths). Consider DPQC architectures in which (a) the only nonunitary operations are single-qubit feedforward operations as studied in Section 3, (b) there are at most a polynomial number of such feedforward operations, and (c) the parameterized gates are “locally scrambling” as defined in [Ang+24], these DPQC architectures can be efficiently classically simulated with high probability with respect to the distribution of parameters via the low weight Pauli paths algorithm of [Ang+24].

While the DPQC architectures from Observation 4 are not explicitly considered in [Ang+24], one can extract the observation above from the following reasoning. Firstly, as noted in Appendix A, we can replace each nonunitary operation with an ancilla qubit and some unitary interactions between this ancilla qubit and the wire on which the feedforward operation takes place—i.e. we can replace the feedforward with a unitary “feedforward gadget” in the purified picture, at the cost of at most two ancillas per feedforward operation. Given that the local scrambling property is satisfied by assumption, we can now apply the algorithm of [Ang+24] to this circuit. The requirement that there are at most a polynomial number of feedforward operations is to ensure that at most polynomially many ancilla qubits are added. Next we note that each feedforward gadget does not increase the weight of a propagated Pauli string on the system qubits. While the Pauli strings can spread on to the ancilla qubits,

since only identity operations happen on ancilla qubits after a gadget, they can be easily handled.

At first glance, one might think that Observation 4 renders those DPQC architectures unsuitable for variational quantum algorithms which hope to offer some advantage over classical methods. However, this is not the case. More specifically, as shown in Figure 10, even if a circuit architecture is average-case easy to simulate, it could still be the case that there exist meaningful and relevant problems for which variational quantum algorithms encounter hard instances during execution, and therefore *cannot* be efficiently classically simulated, despite the average-case simulability.

Finally, before moving on to the question of whether or not hard instances occur during optimization, we make some brief comments on the *limitations* of the low-weight Pauli paths algorithm from [Ang+24]. In particular, we note that this algorithm works in the Heisenberg picture, by backwards evolving an observable through the quantum circuit (while keeping track of a suitably truncated Pauli expansion of the observable). As such, while this algorithm can provide expectation values of observables, it cannot provide a succinct representation of the output state of the quantum circuit. Given this, for the large majority of target applications of VQAs, where what one wants is the expectation value of local observables, the low-weight Pauli paths algorithm is sufficient. However one could also imagine situations where one desires a description of the output state of the circuit (for instance, to perform phase estimation), and in this case the low-weight Pauli paths algorithm would not be sufficient.

6.3 Do hard instances occur during optimization?

Given the discussion at the end of the previous section, and following the methodology of Figure 10, we study here the question of whether or not there exist meaningful problems for which variational quantum algorithms using dynamic parameterized quantum circuits encounter hard instances for classical simulation during their execution. More specifically, we are particularly interested in the case when:

1. The PQC architecture is barren plateau free.
2. The PQC architecture is also efficiently classically simulable on average.
3. The VQA is only allowed to make a polynomial number of measurements and run for polynomial time.

In order to lay the foundations for such a discussion it is necessary for us to characterize to some extent which circuit instances could be reached during execution of a variational quantum algorithm. We stress that, as per the list above, to be practically meaningful we restrict ourselves to VQAs which use at most polynomial time and measurements. With this in mind, let us imagine that on initialization, or during optimization, a polynomially-constrained VQA reaches a circuit instance for which all loss function gradients are exponentially small (which we refer to as negligible). There are now two options: The first option is to take enough measurements to resolve the gradient to an accuracy which allows for a meaningful parameter update (i.e. one which has some guarantee of leading to a decrease in the loss). Unfortunately, this is not possible within the polynomial resource constraint. The second option is to use only a polynomial number of measurements to estimate the gradient. In this case however, the estimated gradient is essentially random, and the subsequent update is therefore essentially a guess, as opposed to a meaningful optimization step.

Given the observations above, we see that if we restrict ourselves to polynomially constrained VQAs, which only make *meaningful* parameter updates, then we can assume that such VQAs only explore/reach circuit instances with non-negligible gradients. More specifically, when such an algorithm encounters an instance with a negligible gradient, it has to either stop, or guess a parameter update. We reiterate that there certainly are polynomially constrained VQAs which can reach *any* point in parameter space—consider for example a VQA that just updates parameters by guessing new parameters randomly—however such VQAs must at some point perform poorly-motivated or random parameter updates, and we do not expect them to succeed in cost function minimization. As such, from now on

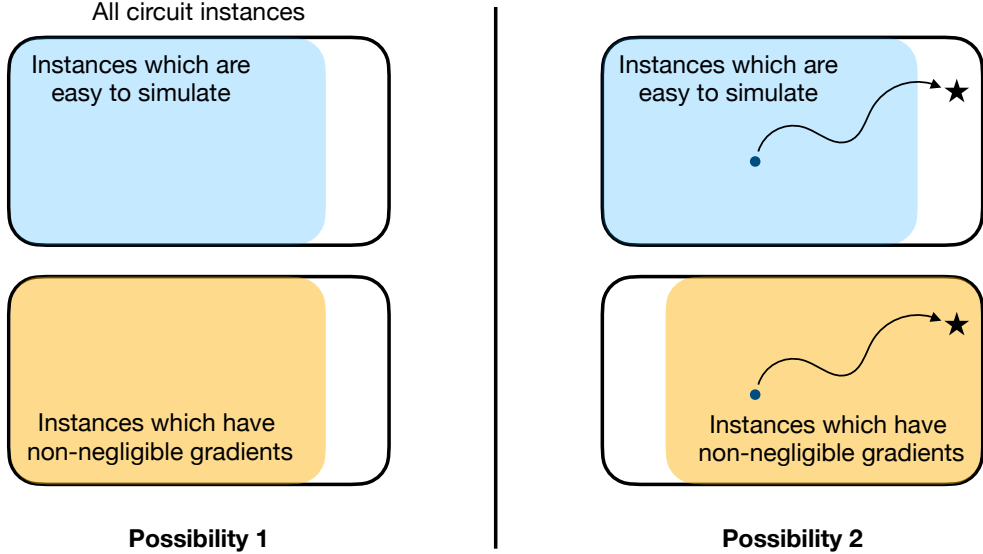


Figure 11: An illustration of two different possibilities for the distribution of circuit instances with non-negligible gradients and the distribution of instances which are easy to simulate, for circuit architectures which are barren plateau free. Which of these possibilities is true has consequences for whether or not classical hard instances are likely to occur during a variational quantum algorithm. This is discussed in Section 6.3.

we will restrict ourselves to meaningful (in the sense explained above) polynomially constrained VQAs, which we assume can only explore/reach circuit instances with non-negligible gradients.

Given this assumption, in order to understand whether or not a meaningful polynomially constrained VQA can reach hard-to-simulate instances, we would like to characterize the classical simulability of those circuit instances with non-negligible gradients. In particular, if *all* such instances are efficiently classically simulable, then clearly, under our assumptions on the VQA, no classically hard instances can occur during polynomial time optimization!

For the case of interest in which the PQC architecture is both barren plateau free, and efficiently classically simulable on average, the situation is illustrated in Figure 11. In particular, the absence of barren plateau result implies that *some* large fraction of instances do have non-negligible gradients, and are therefore reachable under our assumptions. Simultaneously, the average-case simulation result implies that *some other* large fraction of instances can be efficiently classically simulated. The important question is then how these fractions of instances are related to each other, and there are two distinct possibilities:

1. **Possibility 1:** All instances that have non-negligible gradients (and are therefore reachable) are easy to efficiently simulate classically.
2. **Possibility 2:** There exist instances that have non-negligible gradients (and are therefore reachable), which are hard to efficiently simulate classically.

Note that if the first possibility is true, then this rules out the utility of running variational quantum algorithms with these architectures on quantum devices, for any problem where local expectation values of the target state are the desired outcome. If possibility 2 is true, this implies that VQAs *could* potentially reach hard instances during optimization, but *does not* imply that they will always reach hard instances in practice. So which of these two possibilities is the case?

On the one hand, one could reasonably conjecture that possibility 1 is the case, because the mechanism which makes a particular instance efficient to classically simulate (low weight Pauli path) is very similar to the mechanism which leads to non-negligible gradients (as discussed in Section 4.5). We view formalizing this connection, between efficient simulation via suppression of high weight Pauli

paths and non-negligible gradients via suppression of high S-weight strings in the stat-mech model, as an important and immediate open problem. Additionally, we note that [Cer+23] has accumulated evidence for the truth of this conjecture for certain PQC architectures, by reasoning about properties of an architecture’s dynamical lie algebra (DLA), which is also intimately linked to both non-negligible gradients and efficient classical simulations. However, this DLA picture is not immediately applicable to the dynamic parameterized quantum circuit architectures we study in this work, and as such we view understanding the relation between barren plateaus in the stat-mech picture and classical simulations via Pauli path propagation as crucial to the larger project of understanding the extent to which “absence of barren plateaus implies classical simulability” [Cer+23].

On the other hand, the numerical experiments we presented in Section 5 provide some evidence that possibility 2 might be true. More specifically, in the discussion of worst-case hardness given in Section 6.1, we argued that DPQC architectures are worst-case hard to simulate because they contain poly-depth *unitary* architectures (which produce pure states). However, because DPQC architectures are generically nonunitary by design, one might intuitively and justifiably expect that VQAs using DQPC architectures never converge in practice to unitary circuits, and therefore never have a chance of reaching the instances we used to prove worst-case hardness. However, we have seen in Section 5 that for a meaningful problem, VQAs with DPQC architectures *can* indeed converge to unitary circuits which prepare pure states! Of course, not all unitary instances are hard to simulate—in particular, the ground state of the model considered in Section 5.1 can be efficiently prepared and represented classically! As such, the numerical results from Section 5 *do not* prove that possibility 2 is the case, but provide evidence to believe that VQAs with DPQCs might be able to reach instances that are structurally more similar to the (pure) worst-case hard instances than (impure) generic states for which average-case easiness holds.

We do, however, reiterate the caveats and criticisms from Section 5.3. In particular, the numerical experiments from Section 5 have been performed for relatively small instances, with no shot noise or circuit noise. As such, any evidence derived from these results needs to be treated cautiously. In particular, one could argue that by not including shot noise, we have included in our numerical simulations algorithms that can make exponentially many measurements.

In summary, it is as of yet unclear whether possibility 1 or 2 is the case when using variational quantum algorithms with dynamic parameterized quantum circuit architectures for meaningful problems. Above, we have sketched two potential routes for resolving this issue, which we believe are concrete and important avenues for future research.

7 Outlook and conclusions

This work focuses on a *dynamic* parameterized quantum circuit class that is constructed by unitary gates, intermediate measurements, and feedforward operations. The study was motivated by the question of whether this circuit class provides a *good* ansatz for variational quantum algorithms. This presents a particularly important question given that most known variational quantum ansatz classes suffer from drawbacks which result in them being either untrainable, classically simulable, or insufficiently expressive. More specifically, we are looking for an ansatz that may offer an avenue for training scalable variational quantum algorithms, capable of finding good solutions to interesting problems, and challenging for classical computers.

Our theoretical analysis indicates that the studied DPQC class corresponds to a *promising* model for variational quantum algorithms. Evidence for this intuition comes from the fact that DQPC models can be both expressive and free from barren plateaus. Specifically, we have shown that one can construct DPQC models which contain arbitrarily deep unitary quantum circuits—and are therefore worst case hard to simulate classically—while at the same time not suffering from exponentially vanishing gradients. These models can interpolate smoothly between being highly expressive and barren plateau

free, making them a convenient design choice. We stress, however, that absence of barren plateaus does not imply trainability, and it remains an open question whether worst-case hard instances for classical simulation can be encountered during the training of DPQC models, if one is allowed only polynomially many resources (measurements, time) for training.

The potential of the DPQC is additionally supported by numerical experiments on ground state and thermal state preparation problems with the former confirming our theoretical insights and the latter indicating applicability beyond the analytically studied setting. While the numerical results demonstrate the capability to learn interesting models, it remains an open task for future research to investigate whether the observed good training behavior persists for larger system sizes. Additionally, in order to reliably argue about the capabilities of our ansatz for thermal state preparation, it remains to be investigated whether the thermal state experiments may be reproduced with scalable cost functions [ZLW21; WLW21].

The DPQC provides a promising model that is worth studying in future research. Answering the open questions about trainability and classical simulability outlined above are crucial steps towards understanding its *quantum utility*.

Author contributions. AD: Conceptualization, Software, Formal analysis, Investigation, Writing–Original Draft, Supervision. MH: Writing–Review and Editing. SN: Writing–Review and Editing. KS: Writing–Review and Editing. RS: Conceptualization, Writing–Original Draft, Writing–Review and Editing, Supervision. CZ: Conceptualization, Software, Investigation, Writing–Review and Editing.

Acknowledgments. We acknowledge discussions with Zoë Holmes, Manuel S. Rudolph, and Armando Angrisani.

A Definitions and Notation

We set up here a few notations and recap some definitions from the main text. We work with quantum circuits composed of two-qubit gates over n qubits with a total depth d . The total number of gates is denoted m . We denote the space of Hermitian observables on n qubits $\text{Herm}(n)$. The space of valid density matrices on n qubits, or equivalently, the space of positive semidefinite trace 1 Hermitian matrices is $\text{Dens}(n) \subset \text{Herm}(n)$. We consider circuits with nonunitary operations, which we describe through channels, denoted by calligraphic letters such as $\mathcal{U}(\rho_{\text{init}}) : \text{Dens}(n) \rightarrow \text{Dens}(n)$.

In some calculations, we take t copies of a state, which means studying the object where the initial state is $\rho_{\text{init}}^{\otimes t}$ and applying copies of the unitary channel on the initial state: $\mathcal{U}^{\otimes t}(\rho_{\text{init}}^{\otimes t})$. Let \mathbb{S}_t be the permutation group on t objects labeled by integers $[t]$, with group elements $\sigma : [t] \rightarrow [t]$. Consider a representation of \mathbb{S}_t where each permutation σ is associated with the map that permutes copies of quantum states through conjugation, i.e. $R(\sigma)(\cdot)R(\sigma)^\dagger : \text{Dens}(n \times t) \rightarrow \text{Dens}(n \times t)$. The symmetric subspace P^t is defined by operators $\{O : R(\sigma)OR(\sigma)^\dagger = O\}$ invariant under permutations $\sigma \in \mathbb{S}_t$.

For $t = 2$, the group \mathbb{S}_2 has the elements identity e and SWAP s , satisfying

$$e(1) = 1; \quad s(1) = 2 \tag{27}$$

$$e(2) = 2; \quad s(2) = 1. \tag{28}$$

The representation of these elements for 1-qubit density matrices is $R : \text{Dens}(2) \rightarrow \text{Dens}(2)$, which has elements

$$R(e) = I = \begin{array}{c} \text{---} \\ \text{---} \end{array}, \tag{29}$$

$$R(s) = S = \begin{array}{c} \diagup \diagdown \\ \text{---} \end{array}. \tag{30}$$

Definition 5 (Haar measure). The Haar measure \mathcal{H} on the unitary group $U(N)$ is the unique probability measure that is both left and right invariant under the group action. That is, for any integrable function

f and for all $V \in \mathrm{U}(N)$, it holds that

$$\int_{U \in \mathrm{U}(N)} f(U) d\mathcal{H}(U) = \int_{U \in \mathrm{U}(N)} f(UV) d\mathcal{H}(U) = \int_{U \in \mathrm{U}(N)} f(VU) d\mathcal{H}(U). \quad (31)$$

In this work, we are interested in systems of n qubits such that we consider $N = 2^n$.

Definition 6 (Unitary t -design). Let \mathcal{E} be an ensemble of n -qubit unitaries. Then, \mathcal{E} is a unitary t -design if and only if for all $O \in \mathcal{L}((\mathbb{C}^2)^{\otimes n})^{\otimes t}$, it holds that

$$\mathbb{E}_{V \sim \mathcal{E}}[V^{\otimes 2} O V^\dagger]^{\otimes t} = \mathbb{E}_{V \sim \mathcal{H}}[V^{\otimes 2} O V^\dagger]^{\otimes t}. \quad (32)$$

In the following, for any Haar averages like the one on the RHS of Equation (32), we will usually omit the explicit mentioning of \mathcal{H} and simply write \mathbb{E}_V .

We denote by \mathbb{P}_n the set of all Pauli observables on n qubits and by α a particular Pauli observable indexed by α . We now recall our definition of dynamic operations.

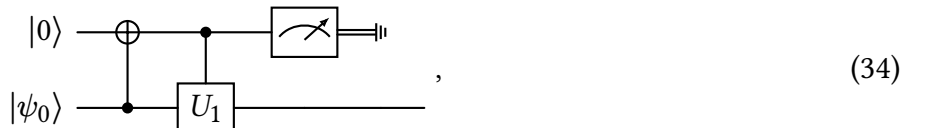
Definition 7 (Dynamic operation). A dynamic operation is a quantum channel that may be implemented via a projective measurement followed by a future operation conditioned on the measurement result.

As an example, the simplest nontrivial dynamic operation is the following:



Here, the state is measured, followed by a conditional gate U_1 if the measurement result was 1 and I otherwise.

It is often convenient to view these operations in a larger Hilbert space by introducing an ancilla to record the intermediate measurement results and converting the conditional statements into gates that condition on the ancilla. We call this the purified picture. Concretely, the purified picture of the above feedforward operation is:



where we trace out the ancilla after measurement. (Hence, strictly speaking, the measurement on the ancilla is superfluous.) We fix

$$U_1 = \begin{pmatrix} \cos \varphi e^{-i\phi} & -i \sin \varphi \\ -i \sin \varphi & \cos \varphi e^{i\phi} \end{pmatrix}. \quad (35)$$

Recall the definition of a parameterized dynamic circuit:

Definition 8 (Parameterized dynamic circuit). A parameterized dynamic circuit \mathcal{C} of depth- d on an architecture is a sequence of channels $\{\mathcal{U}_1(\boldsymbol{\theta}), \mathcal{U}_2(\boldsymbol{\theta}), \dots, \mathcal{U}_d(\boldsymbol{\theta})\}$, where each channel $\mathcal{U}_j(\boldsymbol{\theta}) : \mathrm{Dens}(n) \rightarrow \mathrm{Dens}(n)$ is a completely positive, trace preserving map on n qubits that describes the operations in time step j . The operations in each layer j can be written as a composition of single- and two-qubit operations such that the two-qubit operations act on non-overlapping qubits and only connect qubits with an edge in the associated graph describing the circuit architecture. The parameters $\boldsymbol{\theta}$ come from a set $\Theta \in \mathbb{R}^p$ for $p \in \mathrm{poly}(n)$. The action of the entire circuit is described by the channel $\mathcal{C}(\boldsymbol{\theta}) = \mathcal{U}_d(\boldsymbol{\theta}) \circ \dots \circ \mathcal{U}_1(\boldsymbol{\theta})$.

In the most general case in this definition, some operations in the circuit may depend on no parameters, and some parameters may influence multiple operations. For simplicity, we focus on the case where each parameter θ is a rotation angle of either a single-qubit gate $e^{-i\theta\sigma}$ or a two-qubit gate $e^{-i\theta\sigma\otimes\sigma}$ for some Pauli matrix σ , and each parameter only controls a single gate.

We also need the idea of the effective channel up to time i :

Definition 9. The effective channel until time i is given by $\mathcal{C}_i = \mathcal{U}_i(\boldsymbol{\theta}) \circ \dots \circ \mathcal{U}_1(\boldsymbol{\theta})$.

With this in hand, we now define the ensemble of circuits we work with.

Definition 10 (Ensemble of dynamic circuits). Suppose there is a probability distribution \mathcal{D}_p defined on the space of possible parameter values Θ . This distribution induces in a natural way a distribution over $\mathcal{C}(\boldsymbol{\theta})$ by choosing $\boldsymbol{\theta} \sim \mathcal{D}_p$. We denote this ensemble of dynamic circuits, and equivalently, channels, \mathcal{B} .

We are interested in ensembles of dynamic circuits \mathcal{B} which have the property that the distribution over every operation is invariant under a single-qubit rotation chosen from a 2-design ensemble. Equivalently, we may assume the parameterized circuit has the form $\mathcal{C} = \mathcal{V}_d(\boldsymbol{\theta})\mathcal{U}_d(\boldsymbol{\theta}) \circ \dots \mathcal{V}_1(\boldsymbol{\theta}) \circ \mathcal{U}_1(\boldsymbol{\theta})$, where $\mathcal{V}_1(\boldsymbol{\theta})(\rho) = (\prod_{i=1}^n V_i(\boldsymbol{\theta})) \rho (\prod_{i=1}^n V_i(\boldsymbol{\theta}))^\dagger$ is a product of single-qubit unitaries $V_i \sim \mathcal{T}_2$ for a suitable 2-design \mathcal{T}_2 .

We define here a few quantities that will be useful in our analysis.

Definition 11 (Backwards light cone). Consider a parameterized dynamic circuit. For a subregion $A \subset [n]$, define G_d to be the set of operations in \mathcal{U}_d that can potentially affect the subregion, i.e. satisfy $\text{supp}(G_d) \cap A \neq \emptyset$. Recursively define $G_{j-1} = \{G \in \mathcal{U}_{j-1} : \text{supp}(G) \cap G_j \neq \emptyset\}$. The depth k -backwards light cone of A is the set $L_k^b(A) := G_d \cup G_{d-1} \dots G_{d-k}$. Proceeding to depth 1, the set $L^b(A) := G_d \cup G_{d-1} \dots G_1$ is called the backwards light cone of the subregion A .

Definition 12 (Path). A path in a circuit originating from time t is a specification of space-time locations, i.e. a choice of a qubit $\ell(i) \forall i \in \{t, t+1, \dots, d\}$, such that for every time slice i , there is a gate or operation in \mathcal{U}_i that connects $\ell(i)$ and $\ell(i+1)$, meaning that the operation is supported both on qubits $\ell(i)$ and $\ell(i+1)$. We denote such a path using its beginning and end points $p(\ell(t), \ell(d))$.

Definition 13 (Path length). The length of a path $p(\ell(t), \ell(d)) = (\ell(t), \ell(t+1), \dots)$ is the number of space-time locations j such that in the associated circuit, the operation from \mathcal{U}_j that acts on $\ell(j)$ and $\ell(j+1)$ is an entangling gate. We denote the length of a path $|p(\ell(t), \ell(d))|$.

Definition 14 (Worst-case feedforward distance). Consider paths arising from any feedforward operation at any time t and ending in qubit j and define the feedforward distance of qubit j to be the minimum path length of all these paths. Now, consider the maximum feedforward distance out of all qubits $j \in [n]$. We define this to be the worst-case feedforward distance of the parameterized dynamic circuit, denoted f . More precisely,

$$f = \max_{j \in [n]} \min_{\ell(t): \text{feedforward}} |p(\ell(t), j)|. \quad (36)$$

B The stat-mech model

We derive the basics of the technique here. Our discussion closely follows that of [Hun19; DHB20; DHB21; Nap22]. The first observation that enables the stat-mech model mapping is the “replica trick”:

$$\begin{aligned} (\text{Tr } \rho O)^t &= \text{Tr } \rho^{\otimes t} O^{\otimes t} \\ \implies \mathbb{E}_{\mathcal{B}} \left[(\text{Tr } \rho O)^t \right] &= \mathbb{E}_{\mathcal{B}} \left[\text{Tr } \rho^{\otimes t} O^{\otimes t} \right]. \end{aligned} \quad (37)$$

Exchanging the order of the expectation and the trace, we get

$$\mathbb{E}_{\mathcal{B}} [(\text{Tr } \rho O)^t] = \text{Tr } \mathbb{E}_{\mathcal{B}} [\rho^{\otimes t}] O^{\otimes t}. \quad (38)$$

Thus, it suffices to know the average t -copy density matrix $\mathbb{E}_{\mathcal{B}} [\rho^{\otimes t}]$.

The next basic fact we need is that performing the Haar-average over single-qubit gates $\mathbb{E}_V[V^{\otimes t} A V^{\dagger \otimes t}]$ for any single-qubit operator $A \in \text{Herm}(1)$ projects it down to the symmetric subspace over t copies:

$$\mathbb{E}_V[V^{\otimes t} A V^{\dagger \otimes t}] \in P^t, \quad (39)$$

where P^t is the symmetric subspace $\{O : \sigma O \sigma^\dagger = O\}$ defined by operators invariant under permutations $\sigma \in \mathbb{S}_t$. When $t = 1$, the above reduces to

$$\mathbb{E}_V[V A V^\dagger] = \text{Tr } A \frac{I}{2}. \quad (40)$$

For $t = 2$, we use as basis elements the 4×4 identity gate I and the SWAP gate

$$S = \begin{pmatrix} 1 & 0 & 0 & 0 \\ 0 & 0 & 1 & 0 \\ 0 & 1 & 0 & 0 \\ 0 & 0 & 0 & 1 \end{pmatrix}. \quad (41)$$

Note that $S^2 = I$ and $\text{Tr } I = 4$, $\text{Tr } S = 2$. We obtain

$$\mathbb{E}_V[V^{\otimes 2} A V^{\dagger \otimes 2}] = aI + bS, \quad (42)$$

where a and b can be obtained by solving the linear equations $\text{Tr } A = 4a + 2b$, $\text{Tr } AS = 2a + 4b$, giving:

$$\mathbb{E}_V[V^{\otimes 2} A V^{\dagger \otimes 2}] = \frac{\text{Tr } A - \frac{1}{2} \text{Tr } AS}{3} I + \frac{\text{Tr } AS - \frac{1}{2} \text{Tr } A}{3} S. \quad (43)$$

For any state ρ , we call the quantity $\mathbb{E}_V[\rho^{\otimes 2}]$ the 2-copy average state. This is the fundamental object of interest for calculating second moment quantities. Henceforth, we will denote the 2-copy average state by $\bar{\rho}$. For an n -qubit state ρ , the two-copy average state resides in $\text{span}(\{I, S\}^n)$. Specifically, using the trace-1 normalized versions of this basis set $I := \frac{I}{4}$, and $S := \frac{S}{2}$ we write the two-copy average state as

$$\bar{\rho} = \sum_{\vec{x} \in \{0,1\}^n} c_{\vec{x}} I^{1-\vec{x}_1} \cdot S^{\vec{x}_1} \otimes \dots \otimes I^{1-\vec{x}_n} \cdot S^{\vec{x}_n}, \quad (44)$$

where $\sum_{\vec{x}} c_{\vec{x}} = 1$. In this way, we can also associate a two-copy average state with a (quasi)-probability distribution \mathcal{D} over bitstrings $\vec{x} \in \{0, 1\}^n$.

Lastly, we use the fact that the channels are drawn independently of each other, which lets us perform the average over many channels in sequence:

Definition 15. For a circuit with initial state ρ_0 , consider $\rho_i(\boldsymbol{\theta}) = \mathcal{U}_i(\boldsymbol{\theta}) \dots \mathcal{U}_2(\boldsymbol{\theta}) \circ \mathcal{U}_1(\boldsymbol{\theta})(\rho_0)$ the state of the system at time step i when fixing the parameters of the circuit $\boldsymbol{\theta}$. The two-copy average state at time i , denoted $\bar{\rho}_i$, is the average two-copy state of $\rho_i(\boldsymbol{\theta})$ according to the distribution $\boldsymbol{\theta} \sim \mathcal{D}_p$ over parameters, or equivalently, according to the distribution \mathcal{B} over channels.

It is easy to see that this average $\mathbb{E}_{\mathcal{B}}$ does not depend on the operations occurring after time step i since they are not in the backwards light cone of ρ_i .

Claim 1. The average 2-copy state $\bar{\rho}_i$ at time i can be obtained from the average $\bar{\rho}_{i-1}$ at time $i-1$.

We have

$$\mathbb{E}_{\mathcal{B}} [(\mathcal{C}_i(\rho_0))^{\otimes 2}] = \mathbb{E}_{\mathcal{U}_1, \mathcal{U}_2, \dots, \mathcal{U}_i} [(\mathcal{U}_i \dots \mathcal{U}_2 \circ \mathcal{U}_1(\rho_0))^{\otimes 2}] \quad (45)$$

$$= \mathbb{E}_{\mathcal{U}_i} \mathbb{E}_{\mathcal{U}_1, \mathcal{U}_2, \dots, \mathcal{U}_{i-1}} [(\mathcal{U}_i(\rho_{i-1}))^{\otimes 2}] \quad (46)$$

$$= \mathbb{E}_{\mathcal{U}_i} [\mathcal{U}_i^{\otimes 2}(\bar{\rho}_{i-1})]. \quad (47)$$

Therefore, in order to get a handle on properties of $\bar{\rho}_d$, the 2-copy average of the circuit output, it suffices to keep track of the average state $\bar{\rho}_i$ in time.

Claim 2 (Linearity). For a two-copy average state $\bar{\rho}$, we can define the reduced density matrix in the usual way by tracing out the appropriate subregion over both copies. By linearity, this coincides with the two-copy average of the reduced density matrix, i.e. $\mathbb{E}_{\mathcal{B}}[(\text{Tr}_A \rho)^{\otimes 2}] = \text{Tr}_{A \times A} \mathbb{E}_{\mathcal{B}} [\rho^{\otimes 2}]$.

These two properties imply that we can obtain a description of the 2-copy average state at time $i+1$ from the one at time i using *local update* rules. Crucially, it suffices to understand the map $\bar{\rho}_i \mapsto \mathbb{E}_{V_1, V_2} [(V_1 V_2 \otimes V_1 V_2) \mathcal{U} \otimes \mathcal{U}(\bar{\rho}_i) (V_1 V_2 \otimes V_1 V_2)^\dagger]$ for Haar-random single-qubit gates $V_1 V_2$ and various channels \mathcal{U} . We will restrict our attention to channels acting on at most two qubits at a time. Suppose the channel \mathcal{U} has the Kraus form $\mathcal{U}(\cdot) = \sum_l K_l(\cdot) K_l^\dagger$. We write this out in tensor notation as

$$\bar{\rho}_{i+1} = \mathbb{E}_{V_1, V_2} \sum_{l, m} \begin{array}{c} \text{Circuit Diagram:} \\ \text{Two input lines } V_1, V_2 \text{ enter from left.} \\ \text{Line } V_1 \text{ splits into } K_l \text{ and } K_m. \\ \text{Line } V_2 \text{ splits into } K_l^\dagger \text{ and } K_m^\dagger. \\ \text{The circuit then consists of:} \\ \text{1. Two qubit lines } V_1^\dagger, V_2^\dagger \text{ (copies of } V_1, V_2\text{) on the right.} \\ \text{2. Two qubit lines } V_1^\dagger, V_2^\dagger \text{ (copies of } V_1, V_2\text{) on the left.} \\ \text{3. Two qubit lines } V_1^\dagger, V_2^\dagger \text{ (copies of } V_1, V_2\text{) on the right.} \\ \text{4. Two qubit lines } V_1^\dagger, V_2^\dagger \text{ (copies of } V_1, V_2\text{) on the left.} \end{array} \quad (48)$$

where the expressions are read left to right (i.e. time flows from center out to each side). The third and fourth qubit lines are the copies of the first and second, and K_l acts as a two-qubit operator on qubits 1 and 2 or their copies 3 and 4.

Claim 3 (Stat-mech update rule). Consider a two-qubit operation \mathcal{U} . Let the reduced two-copy average state on the qubits at time i be $\bar{\rho}_i = a\mathbb{I}\mathbb{I} + b\mathbb{I}\mathbb{S} + c\mathbb{S}\mathbb{I} + d\mathbb{S}\mathbb{S}$. Then the reduced two-qubit average state after application of the channel satisfies $\bar{\rho}_{i+1} = \mathbb{E}_{V_1, V_2} [(V_1 V_2 \otimes V_1 V_2) \mathcal{U} \otimes \mathcal{U}(\bar{\rho}_i) (V_1 V_2 \otimes V_1 V_2)^\dagger] = a'\mathbb{I}\mathbb{I} + b'\mathbb{I}\mathbb{S} + c'\mathbb{S}\mathbb{I} + d'\mathbb{S}\mathbb{S}$, where

$$\begin{pmatrix} a' \\ b' \\ c' \\ d' \end{pmatrix} = T \begin{pmatrix} a \\ b \\ c \\ d \end{pmatrix} \quad (49)$$

for a 4×4 stochastic matrix T . We call T the transfer matrix.

We now state some results on the transfer matrices for some common operations. [War+23] derived general stat-mech rules for fixed two-qubit unitaries in terms of their local unitary invariants, the entangling power and the swapping power.

Claim 4 (Transfer matrices of some gates). For a two-qubit gate, T takes the form

$$T = \begin{pmatrix} 1 & \frac{4\alpha}{5} & \frac{4\alpha}{5} & 0 \\ 0 & 1 - \alpha - \beta & \beta & 0 \\ 0 & \beta & 1 - \alpha - \beta & 0 \\ 0 & \frac{\alpha}{5} & \frac{\alpha}{5} & 1 \end{pmatrix}, \quad (50)$$

with $\alpha \in \left[0, \frac{10}{9}\right]$; $\beta \in \left[-\frac{\alpha}{5}, 1 - \frac{4\alpha}{5}\right]$, subject to the constraint $\beta + \frac{\alpha}{5} \leq \left(\beta + \frac{\alpha}{2}\right)^2$. Furthermore, for Haar-random two-qubit gates, we have $\alpha = 1, \beta = 0$.

We will restrict our attention to transfer matrices T that have nonnegative entries in them. For the two-qubit gate transfer matrix in Eq. (50), this corresponds to requiring $\beta \geq 0, \alpha \leq 1 - \beta$. Recall that the case of Haar-random two-qubit gates is covered by setting $\beta = 0, \alpha = 1$ and is included in this analysis. We now interpret the dynamics of the two-copy average state as a random walk over bitstrings.

First, we observe that the two-copy average state of any product initial state $\bar{\rho}_0, \left(\frac{2}{3}\mathbf{I} + \frac{1}{3}\mathbf{S}\right)^n$, can be interpreted as a probability distribution on strings $\vec{x} \in \{0, 1\}^n$ by taking $\Pr[\vec{x}] = \prod_{i=1}^n \left(\frac{2}{3}\right)^{1-x_i} \left(\frac{1}{3}\right)^{x_i}$. Denote this distribution \mathcal{X}_0 .

Claim 5. There is a one-to-one correspondence between a two-copy average state $\bar{\rho}_i$ and its associated distribution \mathcal{X}_i over n -bit strings.

This claim follows because we can write the vector of probabilities $\vec{p}^i := \Pr_{\mathcal{X}_i} \vec{x}$ as

$$\vec{p}^i = T_i \dots T_2 T_1 \vec{p}^0 \quad (51)$$

for a sequence of appropriate transfer matrices corresponding to that of the sequence of operations $\mathcal{U}_1, \dots, \mathcal{U}_i$. The transfer matrices have nonnegative entries, and so does \vec{p}^0 , implying \vec{p}^i has nonnegative components. Furthermore,

$$\sum_j \vec{p}_j^i = \sum_{j,k} (T_i)_{jk} \vec{p}_k^{i-1} = \sum_k \vec{p}_k^{i-1} \quad (52)$$

since the matrix T_i is stochastic. Proceeding inductively, we get $\sum_j \vec{p}_j^i = \sum_j \vec{p}_j^0 = 1$. Therefore, \vec{p}^i is a probability distribution.

For the rest of this section, we will illustrate the physics of the model by considering Haar-random two-qubit gates as an example. However, recall that the analysis also holds for arbitrary two-qubit gates as long as they are followed by random single-qubit gates from a 2-design. We will state a fact on the steady state of the two-copy average:

Claim 6 (Convergence to global Haar average [DHB20]). For a sufficiently well-connected architecture, in the limit $d \rightarrow \infty$, the two-copy average state $\bar{\rho}_d$ converges to

$$\lim_{d \rightarrow \infty} \bar{\rho}_d = \bar{\rho}_H = \frac{2^n}{2^n + 1} \mathbf{II} \dots \mathbf{I} + \frac{1}{2^n + 1} \mathbf{SS} \dots \mathbf{S}. \quad (53)$$

This is the same two-copy average as that of a global Haar-random state on n qubits. This fact gives barren plateaus for deep random quantum circuits on any architecture, since one can often show for certain architectures that the convergence is exponentially fast in the depth. Morally speaking, for unitary random circuits, any second moment quantity such as the variance of the loss function, is close to that of global Haar-random unitaries for sufficient depth. The global Haar-average state $\bar{\rho}_H$ and the identity state $\mathbf{II} \dots \mathbf{I}$ are the two fixed points under random local unitaries.

Claim 7 (Noisy update rules). In the presence of noise, which we model as local stochastic noise acting on every qubit after every layer of gates, there is an additional stat-mech rule. We have [DHB21]

$$T_{\text{noise}} = \begin{pmatrix} 1 & \gamma \\ 0 & 1 - \gamma \end{pmatrix}, \quad (54)$$

where γ is proportional to the average infidelity of the noise channel. For nonunital single-qubit noise channels, we have [War+23]

$$T_{\text{noise}} = \begin{pmatrix} 1 - \delta & \gamma \\ \delta & 1 - \gamma \end{pmatrix}, \quad (55)$$

for parameters $\delta \leq \gamma$ related to the nonunitality and the nonunitarity of the channel.

B.1 Connection between the stat-mech model and barren plateaus

Assume the loss function is given by $L(\boldsymbol{\theta}) = \text{Tr } \rho(\boldsymbol{\theta})H$, where $H = \sum_i h_i$ is a Hermitian observable and the individual ‘‘terms’’ h_i of H , are operators in $\text{Herm}(n)$ of locality at most k , i.e., can be written as $h_i = \tilde{h}_A \otimes I_{A^c}$ for a subset A of size at most k . We can assume without loss of generality that $\text{Tr } H = 0$. We are usually interested in terms of constant locality $k = O(1)$ and constant norm, since for these observables, we can estimate $\text{Tr } \rho h_i$ to additive error ϵ using $O(1/\epsilon^2)$ copies of ρ with high probability.

When studying barren plateaus, we are interested in the typical variance of the cost function when initializing the parameters $\boldsymbol{\theta}$ randomly from a distribution \mathcal{D}_p .

Lemma 5 (Variance in terms of marginal distribution). Consider a k -local Hamiltonian $H = \sum_{\boldsymbol{\alpha} \in \mathbb{P}_n} c_{\boldsymbol{\alpha}} \boldsymbol{\alpha}$ and a parameterized dynamic quantum circuit \mathcal{C} taking in parameters $\boldsymbol{\theta} \in \Theta$. For a probability distribution \mathcal{D}_p over Θ the set of circuit parameters such that each component $\boldsymbol{\theta}_i$ of $\boldsymbol{\theta}$ controls the parameter of a single operation in \mathcal{C} and is invariant under single-qubit random gates from a 2-design inserted after every gate, the variance of the loss function $L = \text{Tr } \rho(\boldsymbol{\theta})H$ is given by

$$\underset{\boldsymbol{\theta} \sim \mathcal{D}_p}{\text{Var}} L = \sum_{\boldsymbol{\alpha}} c_{\boldsymbol{\alpha}}^2 \Pr_{\mathcal{X}_d}[\vec{x}_{\text{supp}(\boldsymbol{\alpha})} = 11 \dots 1_{\text{supp}(\boldsymbol{\alpha})}], \quad (56)$$

where the probability on the RHS can be understood as the probability, when drawing a bit string \vec{x} from the distribution over bitstrings \mathcal{X}_d at time d , that all of the entries of the \vec{x} corresponding to qubits on which $\boldsymbol{\alpha}$ is supported are equal to 1.

Proof. We have

$$\mathbb{E}_{\boldsymbol{\theta} \sim \mathcal{D}_p} \text{Var } L = \mathbb{E}_{\boldsymbol{\theta} \sim \mathcal{D}_p} [L(\boldsymbol{\theta})^2] - (\mathbb{E}_{\boldsymbol{\theta} \sim \mathcal{D}_p} [L(\boldsymbol{\theta})])^2 \quad (57)$$

$$= \mathbb{E}_{\mathcal{B}} [(\text{Tr } \rho H)^2] - (\mathbb{E}_{\mathcal{B}} [\text{Tr } \rho H])^2. \quad (58)$$

We can rewrite the Hamiltonian in terms of a traceless part H' and a part proportional to the identity λI . The latter portion does not contribute to the variance, so we focus on the traceless portion (and denote it H for the rest of the proof). The second term yields

$$(\mathbb{E}_{\mathcal{B}} [\text{Tr } \rho H])^2 = (\text{Tr } \mathbb{E}_{\mathcal{B}} [\rho H])^2 \quad (59)$$

$$= (\text{Tr } \mathbb{E}_{\mathcal{B}} [\rho] H)^2 \quad (60)$$

$$= \left(\text{Tr } \frac{H}{2^n} \right)^2 \quad (61)$$

$$= 0 \quad (62)$$

for any distribution with a final layer of single-qubit gates from a one-design. We now focus on the quantity $\mathbb{E}_{\mathcal{B}} [(\text{Tr } \rho H)^2]$. This quantity can be expressed in terms of the average two-copy state

$$\mathbb{E}_{\mathcal{B}} [(\text{Tr } \rho H)^2] = \mathbb{E}_{\mathcal{B}} [\text{Tr } \rho^{\otimes 2} \cdot H^{\otimes 2}] = \text{Tr } \bar{\rho} \cdot H^{\otimes 2} \quad (63)$$

as seen before.

Since the two-qubit gates are from an ensemble invariant to single-qubit gates from a 2-design, we assume that the single-qubit gates are independently drawn according to the Haar measure \mathcal{H} . The two calculations coincide because we are computing a second moment quantity over the ensemble. We find that it is often convenient to insert an additional (virtual) layer of random single-qubit unitaries $V_n \sim \mathcal{H}$ at the end of the circuit and Heisenberg-evolve the output observable:

$$\mathbb{E}_{\mathcal{B}} \left[\text{Tr} \rho^{\otimes 2} \cdot H^{\otimes 2} \right] = \mathbb{E}_{\mathcal{B}} \mathbb{E}_{V_n \sim \mathcal{H}} \left[\text{Tr} \rho^{\otimes 2} (V_n \otimes V_n)^\dagger H^{\otimes 2} (V_n \otimes V_n) \right]. \quad (64)$$

We now perform the Haar-average over each single-qubit gate V_{nk} in $V_n = \bigotimes_k V_{nk}$. Recall from Eq. (43) that a single-qubit non-identity Pauli averages to:

$$\mathbb{E}_{V_{nk} \sim \mathcal{H}} [V_{nk}^{\otimes 2\dagger} \boldsymbol{\alpha}^{\otimes 2} V_{nk}^{\otimes 2}] = \frac{\text{Tr } \boldsymbol{\alpha}^{\otimes 2} - \frac{1}{2} \text{Tr } \boldsymbol{\alpha}^{\otimes 2} S}{3} I + \frac{\text{Tr } \boldsymbol{\alpha}^{\otimes 2} S - \frac{1}{2} \text{Tr } \boldsymbol{\alpha}^{\otimes 2}}{3} S \quad (65)$$

$$= \text{Tr } \boldsymbol{\alpha}^2 \times \left(\frac{-1}{6} I + \frac{1}{3} S \right) \quad (66)$$

$$= \frac{-4}{3} I + \frac{4}{3} S. \quad (67)$$

When generalizing this to the n -qubit Haar-average over V_n , we choose to arrange the qubits in our notation according to the partition into $\text{supp}(\boldsymbol{\alpha})$ and its complement.

$$\mathbb{E}_{V_n \sim \mathcal{H}^n} \left[(V_n \otimes V_n)^\dagger \boldsymbol{\alpha}^{\otimes 2} (V_n \otimes V_n) \right] = \bigotimes_{i \notin \text{supp}(\boldsymbol{\alpha})} 4I_i \bigotimes_{j \in \text{supp}(\boldsymbol{\alpha})} \frac{4}{3}(S - I)_j, \quad (68)$$

$$= \frac{4^n}{3^{|\boldsymbol{\alpha}|}} I^{\otimes(n-|\boldsymbol{\alpha}|)} \otimes (S - I)^{\otimes|\boldsymbol{\alpha}|}. \quad (69)$$

In particular, in the last line, we have arranged the qubit indices so that the qubits in the support of $\boldsymbol{\alpha}$ appear last. Furthermore, $|\boldsymbol{\alpha}|$ denotes the weight of the Pauli word $\boldsymbol{\alpha}$.

Continuing to calculate $\mathbb{E}_{\mathcal{B}} \left[\text{Tr} \rho^{\otimes 2} H^{\otimes 2} \right]$, we have

$$\mathbb{E}_{\mathcal{B}} \left[\text{Tr} \rho^{\otimes 2} H^{\otimes 2} \right] = \sum_{\boldsymbol{\alpha}, \boldsymbol{\beta} \in \mathbb{P}_n} c_{\boldsymbol{\alpha}} c_{\boldsymbol{\beta}} \mathbb{E}_{\mathcal{B}} \left[\text{Tr} \rho^{\otimes 2} \cdot \boldsymbol{\alpha} \otimes \boldsymbol{\beta} \right] \quad (70)$$

$$= \sum_{\boldsymbol{\alpha}} c_{\boldsymbol{\alpha}}^2 \mathbb{E}_{\mathcal{B}} \left[\text{Tr} \rho^{\otimes 2} \cdot \boldsymbol{\alpha} \otimes \boldsymbol{\alpha} \right], \quad (71)$$

since if $\boldsymbol{\alpha} \neq \boldsymbol{\beta}$, we will have $\text{Tr}(\boldsymbol{\alpha} \otimes \boldsymbol{\beta}) = 0$ and $\text{Tr}(\boldsymbol{\alpha} \otimes \boldsymbol{\beta} \cdot S) = 0$, giving $\mathbb{E}_{V_n \sim \mathcal{H}} [\boldsymbol{\alpha} \otimes \boldsymbol{\beta}] = 0$. Therefore

$$\mathbb{E}_{\mathcal{B}} \left[\text{Tr} \rho^{\otimes 2} H^{\otimes 2} \right] = \sum_{\boldsymbol{\alpha}} \frac{4^n}{3^{|\boldsymbol{\alpha}|}} c_{\boldsymbol{\alpha}}^2 \text{Tr} \left[\bar{\rho} \cdot I^{\otimes(n-|\boldsymbol{\alpha}|)} \otimes (S - I)^{\otimes|\boldsymbol{\alpha}|} \right] \quad (72)$$

Now consider a particular term in Eq. (72). We obtain

$$\mathbb{E}_{\mathcal{B}} \left[\text{Tr} \rho^{\otimes 2} \boldsymbol{\alpha}^{\otimes 2} \right] = \frac{4^n}{3^{|\boldsymbol{\alpha}|}} \text{Tr} \left[\bar{\rho} \cdot I^{\otimes(n-|\boldsymbol{\alpha}|)} (S - I)^{\otimes|\boldsymbol{\alpha}|} \right] \quad (73)$$

$$= \frac{4^n}{3^{|\boldsymbol{\alpha}|}} \text{Tr}_A \text{Tr}_{A^c} \left[\bar{\rho} \cdot I^{\otimes(n-|\boldsymbol{\alpha}|)} (S - I)^{\otimes|\boldsymbol{\alpha}|} \right], \quad (74)$$

where we have split the trace into one over the support of $\boldsymbol{\alpha}$, A , and another on its complement A^c . Let us perform the trace over the complement first. We get a factor of $4^{-n+|\boldsymbol{\alpha}|}$ from the normalization factors of the I operators. Let

$$\text{Tr}_{A^c} \bar{\rho} = \sum_{\vec{x} \in \{0,1\}^{n-|\boldsymbol{\alpha}|}} g_{\vec{x}} I^{\vec{x}_1} S^{1-\vec{x}_1} \dots I^{\vec{x}_n} S^{1-\vec{x}_n}. \quad (75)$$

Now, from the relations

$$\mathrm{Tr} \mathbf{I} \cdot (\mathbf{S} - \mathbf{I}) = 0; \quad \mathrm{Tr} \mathbf{S} \cdot (\mathbf{S} - \mathbf{I}) = \frac{3}{4}, \quad (76)$$

we conclude that each term \vec{x} in $\mathrm{Tr}_{A^c} \bar{\rho}$ when multiplied with $(\mathbf{S} - \mathbf{I})$ gives a trace of 0 unless $\vec{x} = 11 \dots 1$, in which case it yields a trace of 1. This yields a result relating the variance of a term in the loss function to the probability of ending with the all $\mathbf{S}\mathbf{S} \dots \mathbf{S}_{\mathrm{supp}(\alpha)}$ string on the support of that term:

$$\mathbb{E}_{\mathcal{B}} [\mathrm{Tr} \rho^{\otimes 2} \alpha^{\otimes 2}] = g_{11 \dots 1_{\mathrm{supp}(\alpha)}}. \quad (77)$$

Putting everything together, we get

$$\mathrm{Var}_{\theta \sim \mathcal{D}_p} L = \mathbb{E}_{\mathcal{B}} [\mathrm{Tr} \rho^{\otimes 2} H^{\otimes 2}] = \sum_{\alpha} c_{\alpha}^2 g_{11 \dots 1_{\mathrm{supp}(\alpha)}}. \quad (78)$$

□

Note that this lemma is similar to that of Napp [Nap22] except for the fact that we assume arbitrary distributions over 2-qubit gates provided the single-qubit gates are randomly chosen from a 2-design; whereas Napp assumes that the 2-qubit gates are drawn Haar randomly. It is also possible to generalize this result to qudits of dimension q , although for simplicity, we fix $q = 2$ in this work.

B.2 Stat-mech mapping rules for circuits with feedforward operations

In this section, we derive the stat-mech rule for measurements with feedforward operations.

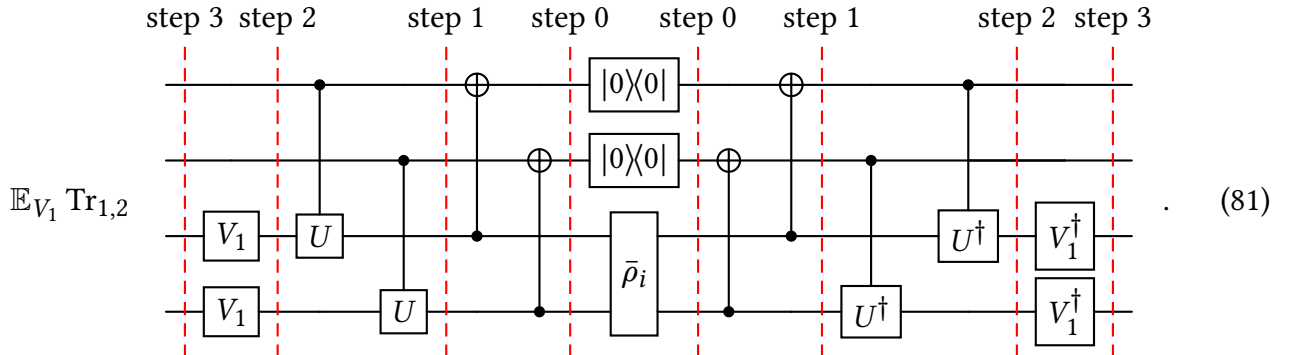
Lemma 6 (Transfer matrix for feedforward operation). For the single-qubit feedforward gadget shown in Eq. (33), the transfer matrix is

$$T_F = \begin{pmatrix} 1 - \frac{\sin^2 \varphi}{3} & \frac{2}{3} \\ \frac{\sin^2 \varphi}{3} & \frac{1}{3} \end{pmatrix}. \quad (79)$$

Proof. We will work in the purified picture for simplicity, where the feedforward gadget is given by Eq. (34). We need to calculate

$$\bar{\rho}_{i+1} = \mathbb{E}_{V_1} [(V_1 \otimes V_1) \mathcal{F} \otimes \mathcal{F}(\bar{\rho}_i) (V_1 \otimes V_1)^\dagger] \quad (80)$$

for Haar-random single-qubit gates V_1 and the feedforward channel \mathcal{F} . The tensor network diagram for this calculation is:



Here time flows from the center outwards on either side, as denoted by the time slices.

Suppose that the initial 2-copy average state is $\bar{\rho}_i = aI + bS$, where I and S are now the unnormalised identity and SWAP operators. Then, the state after step 1 when we apply the CNOTs from lines 3 → 1, 4 → 2 is

$$\begin{aligned} & a(|00\rangle\langle 00| \otimes |00\rangle\langle 00| + |01\rangle\langle 01| \otimes |01\rangle\langle 01| + |10\rangle\langle 10| \otimes |10\rangle\langle 10| + |11\rangle\langle 11| \otimes |11\rangle\langle 11|) \\ & + b(|00\rangle\langle 00| \otimes |00\rangle\langle 00| + |01\rangle\langle 10| \otimes |01\rangle\langle 10| + |10\rangle\langle 01| \otimes |10\rangle\langle 01| + |11\rangle\langle 11| \otimes |11\rangle\langle 11|). \end{aligned} \quad (82)$$

Next, applying the controlled unitary on both copies yields:

$$\begin{aligned} & (a+b)|00\rangle\langle 00| \otimes |00\rangle\langle 00| + (a+b)|11\rangle\langle 11| \otimes (U \otimes U)|11\rangle\langle 11|(U \otimes U)^\dagger \\ & + a|01\rangle\langle 01| \otimes (\sin^2 \varphi |00\rangle\langle 00| - ie^{-i\phi} \sin \varphi \cos \varphi |00\rangle\langle 01| + ie^{i\phi} \sin \varphi \cos \varphi |01\rangle\langle 00| + \cos^2 \varphi |01\rangle\langle 01|) \\ & + a|10\rangle\langle 10| \otimes (\sin^2 \varphi |00\rangle\langle 00| - ie^{-i\phi} \sin \varphi \cos \varphi |00\rangle\langle 10| + ie^{i\phi} \sin \varphi \cos \varphi |10\rangle\langle 00| + \cos^2 \varphi |10\rangle\langle 10|) \\ & + b|01\rangle\langle 10| \otimes (\dots) + b|10\rangle\langle 01| \otimes (\dots), \end{aligned} \quad (83)$$

where we have omitted the last two terms proportional to b because they will vanish when we take the partial trace over the first two qubits. After taking the partial trace, we will have

$$\begin{aligned} & (a+b)|00\rangle\langle 00| + (a+b)(U \otimes U)|11\rangle\langle 11|(U \otimes U)^\dagger \\ & + a(\sin^2 \varphi |00\rangle\langle 00| - ie^{-i\phi} \sin \varphi \cos \varphi |00\rangle\langle 01| + ie^{i\phi} \sin \varphi \cos \varphi |01\rangle\langle 00| + \cos^2 \varphi |01\rangle\langle 01|) \\ & + a(\sin^2 \varphi |00\rangle\langle 00| - ie^{-i\phi} \sin \varphi \cos \varphi |00\rangle\langle 10| + ie^{i\phi} \sin \varphi \cos \varphi |10\rangle\langle 00| + \cos^2 \varphi |10\rangle\langle 10|) \end{aligned} \quad (84)$$

We now perform the average over V_1 . This gives us $\bar{\rho}_{i+1} = \alpha I + \beta S$, where the coefficients can be inferred from

$$\text{Tr } \bar{\rho}_{\text{out}} = 4\alpha + 2\beta = 4a + 2b \quad (85)$$

$$\text{Tr } \bar{\rho}_{\text{out}} S = 2\alpha + 4\beta = 2a + 2b + 2a \sin^2 \varphi \quad (86)$$

$$\implies \alpha = \frac{a(3 - \sin^2 \varphi) + b}{3}, \quad \beta = \frac{2a \sin^2 \varphi + b}{3}. \quad (87)$$

This, in turn, shows that a measurement and feedforward operation leads to the rule for the stat mech model:

$$I \rightarrow \frac{(3 - \sin^2 \varphi)}{3} I + \frac{\sin^2 \varphi}{3} S \quad (88)$$

$$S \rightarrow \frac{2}{3} I + \frac{1}{3} S. \quad (89)$$

□

Let us examine some limits. When $\varphi = 0$, there is no effect of the feedforward unitary and the operation is equivalent to measuring and forgetting the result, or dephasing. The stat mech rule would then be $I \rightarrow I; S \rightarrow \frac{2}{3} I + \frac{1}{3} S$. When $\varphi = \pi/2$, it corresponds to the case of controlled operation being a CNOT, then the whole gadget acts essentially as a reset. In this case, both I and S map to the standard $\frac{2}{3} I + \frac{1}{3} S$ single-qubit average of a pure state. Interestingly, there is no fundamental difference between the stat mech model for any $\varphi > 0$ and $\varphi = \frac{\pi}{2}$.

We can also study the fixed point of this single qubit map for more intuition. We equate $\alpha = a$, $\beta = b = \frac{1}{2} - 2a$ and obtain

$$a = \frac{1}{6 - 2 \cos^2 \varphi}, \quad b = \frac{\sin^2 \varphi}{6 - 2 \cos^2 \varphi}. \quad (90)$$

This again shows that when the measurements only serve to dephase the state ($\varphi = 0$), the fixed point is I , consistent with studies of unital noise [Des+22; War+23], whereas for any nonzero φ , the fixed point of the channel has a nonzero S component.

In sum, we have seen that from the point of view of the second moment and the stat-mech model, there is qualitatively no difference between some $\varphi > 0$, e.g. $\varphi = \frac{\pi}{4}$, and $\varphi = \frac{\pi}{2}$, the case of resets.

B.3 Physics of the feedforward stat-mech model

In this subsection, we will interpret the dynamics of the average two-copy state as a random walk over strings $\{\mathbf{I}, \mathbf{S}\}^n$ and derive our main result, a lower bound on the variance of the loss function.

We have now established the tools and language we need to prove the claimed lower bound on the variance of the loss function.

Lemma 7 (Lower bound on probability mass on \mathbf{S} after feedforward operation). Suppose qubit j undergoes a feedforward operation at time i . Then, the probability that $\vec{x}_j^i = 1$, equivalently, the probability mass $\text{Tr}_{j^c} \bar{\rho}_i \cdot \frac{4}{3}(\mathbf{S} - \mathbf{I})_j$, is lower bounded by $\frac{\sin^2 \varphi}{3}$.

Proof. If $\text{Tr}_{j^c} \bar{\rho}_i = a\mathbf{I} + b\mathbf{S}$, we would like a lower bound on the probability b of seeing an \mathbf{S} after the feedforward operation. From the orthogonality relations in Eq. (76), we get

$$\text{Tr}_{j^c} \bar{\rho}_i \cdot (\mathbf{S} - \mathbf{I})_j = a \cdot 0 + \frac{3}{4}b. \quad (91)$$

This establishes that the quantity $\frac{4}{3} \text{Tr}_{j^c} \bar{\rho}_i \cdot (\mathbf{S} - \mathbf{I})_j$ is the probability mass we desire. As for the lower bound, it follows straightforwardly from observing that Eq. (79) has an entry corresponding to \mathbf{S} of either $\frac{\sin^2 \varphi}{3}$ or $\frac{1}{3}$. Therefore, we get

$$\Pr_{\mathcal{X}_i}[\vec{x}_j^i = 1] = \sum_{k:k_j=1} \vec{p}_k^i \geq \frac{\sin^2 \varphi}{3}, \quad (92)$$

where the sum $\sum_{k:k_j=1}$ plays the role of marginalizing the probability distribution \vec{p}^i over j^c . \square

While this proof is self-evident, this simple fact is crucial. We are able to make a strong statement by giving a constant lower bound on the probability of an event, independent of all other gates in the circuit and independent of the time at which the feedforward operation takes place. Without intermediate measurements and feedforward operations, we typically do not have a good handle on the probability mass on any string or sequence, as seen earlier. As an example, contrast this statement with the following:

Lemma 8 (Lower bound on probability mass on \mathbf{S} surviving after two-qubit gate). Suppose we apply a two-qubit gate on qubits j, j' at time i with transfer matrix parameters α and β following Eq. (50). The conditional probability $\Pr_{\mathcal{X}_i}[\vec{x}_j^i = 1 | \vec{x}_j^{i-1} = 1 \text{ or } \vec{x}_{j'}^{i-1} = 1]$ is lower bounded by $\frac{\alpha}{5}$.

Proof. The proof of this lemma is largely similar to the previous. The main difference is that we are examining the conditional probability of there being an \mathbf{S} on qubit j at time i , with the promise that either qubit j or j' had an \mathbf{S} operator at time $i-1$. In this setting, we can restrict our attention to the columns of the transfer matrix Eq. (50) that correspond to the initial states $\mathbf{IS}_{jj'}, \mathbf{SI}_{jj'}, \mathbf{SS}_{jj'}$, meaning the last three columns of

$$T = \begin{pmatrix} 1 & \frac{4\alpha}{5} & \frac{4\alpha}{5} & 0 \\ 0 & 1 - \alpha - \beta & \beta & 0 \\ 0 & \beta & 1 - \alpha - \beta & 0 \\ 0 & \frac{\alpha}{5} & \frac{\alpha}{5} & 1 \end{pmatrix}. \quad (93)$$

Therefore,

$$\Pr_{\mathcal{X}_i}[\vec{x}_j^i = 1 | \vec{x}_j^{i-1} = 1 \text{ or } \vec{x}_{j'}^{i-1} = 1] \geq \min \left\{ \beta + \frac{\alpha}{5}, 1 - \frac{4\alpha}{5} - \beta, 1 \right\}. \quad (94)$$

Since we have restricted our attention to transfer matrices with nonnegative entries, $\beta \geq 0$ and $\beta \leq 1 - \alpha$. The minimum of the three entries is $\geq \frac{\alpha}{5}$. \square

Informally, Lemma 8 states that an **S** string on a qubit j has a probability at least $\frac{\alpha}{5}$ of remaining at j . By symmetry, we also have the probability that an **S** string on a qubit j moves or spreads to j' after a two-qubit gate on j, j' :

Lemma 9 (Lower bound on probability of **S** hopping or spreading). Suppose we apply a two-qubit gate on qubits j, j' at time i with transfer matrix parameters α and β following Eq. (50). The conditional probability $\Pr_{\mathcal{X}_i}[\vec{x}_{j'}^i = 1 | \vec{x}_j^{i-1} = 1 \text{ or } \vec{x}_{j'}^{i-1} = 1]$ is lower bounded by $\frac{\alpha}{5}$.

Proof. This proof is almost identical and follows from the fact that

$$\Pr_{\mathcal{X}_i}[\vec{x}_{j'}^i = 1 | \vec{x}_j^{i-1} = 1 \text{ or } \vec{x}_{j'}^{i-1} = 1] = \Pr_{\mathcal{X}_i}[\vec{x}_j^i = 1 | \vec{x}_j^{i-1} = 1 \text{ or } \vec{x}_{j'}^{i-1} = 1] \quad (95)$$

since the transfer matrix is symmetric under the operation of exchanging the qubits $j \leftrightarrow j'$. \square

Definition 16 (Circuit-compatible sequence). We call a sequence of bitstrings $\vec{x}^i, \vec{x}^{i+1}, \dots, \vec{x}^j$ a circuit-compatible sequence over $\{\mathbf{I}, \mathbf{S}\}^n$ of a dynamic parameterized circuit \mathcal{C} if they satisfy the consistency condition that the string \vec{x}^l is obtainable in principle from the string at time $l-1$, namely \vec{x}^{l-1} from the sequence of operations in \mathcal{U}_l .

The phrase “obtainable in principle” means that the probability $\Pr_{\mathcal{X}_l}[\vec{x}^l | \vec{x}^{l-1}]$ is nonzero.

Definition 17 (SWAP-active sequence). We call a circuit-compatible sequence “SWAP”-active with respect to a given path if, for all space-time locations $\ell(i)$ specified by the path, we have $\vec{x}_{\ell(i)}^i = 1$.

Informally speaking, a path identifies a potential route from a space-time location with an **S** operator to an **S** operator at the end of the circuit supported on a potentially different location, and we are interested in SWAP-active sequences with respect to this path. Specifically, we would like to lower bound the probability that an **S** operator survives at a given location l at the end of the circuit. This depends on the path length of a path starting from the initial state or a nearby feedforward operation and ending at the given location l .

Lemma 10. Consider a qubit at site l . The probability that the final bitstring contains an **S** at site l , i.e. $\Pr_{\mathcal{X}_d}[\vec{x}_l^d = 1]$, is lower bounded by

$$\frac{\sin^2 \varphi}{3} \left(\frac{\alpha}{5}\right)^{|p(\ell(t), \ell(d))|} \quad (96)$$

for any path starting from a feedforward operation and ending at the site of interest $\ell(d) = l$.

Proof. Consider a path $p(\ell(t), \ell(d))$ starting after a feedforward operation at qubit $\ell(t)$ at time t . This operation results in $\vec{x}_{\ell(t)}^t = 1$ with probability at least $\frac{\sin^2 \varphi}{3}$ from Lemma 7. Once we get a handle on this probability mass, we can lower bound the probability mass of the event $\vec{x}_{\ell(t+1)}^{t+1} = 1$ using the conditional probability lower bounds in Lemmas 8 and 9. If there is an entangling gate between qubits $\ell(t)$ and $\ell(t+1)$ at time $t+1$, then

$$\Pr[\vec{x}_{\ell(t+1)}^{t+1} = 1 | \vec{x}_{\ell(t)}^t = 1] \geq \frac{\alpha}{5}. \quad (97)$$

Otherwise, if the qubit is idle and $\ell(t+1) = \ell(t)$, the probability mass is unaffected. This step holds inductively at arbitrary time slice s :

$$\Pr[\vec{x}_{\ell(s+1)}^{s+1} = 1 | \vec{x}_{\ell(s)}^s = 1] \geq \frac{\alpha}{5}. \quad (98)$$

Chaining together everything, we get

$$\Pr[\vec{x}_{\ell(d)}^d = 1] \geq \Pr[\vec{x}_{\ell(t)}^t = 1] \times \left(\frac{\alpha}{5}\right)^{|p(\ell(t), \ell(d))|}, \quad (99)$$

where we have counted the number of times a two-qubit gate is encountered along the path, which is precisely how we have defined the path length. In order to optimize the lower bound, we look for paths to the closest feedforward or initialization operation, using the distance measure we have defined. The intuition we have made rigorous is that qubit initializations and measurement and feedforward operations are “sources” of \mathbf{S} probability mass. The path between the source and the “sink” (the final destination at l) is a “leaky pipe” where the probability of some mass surviving can decay exponentially in the length of the pipe. Thus, in order to get a good flow rate to the sink, we try and optimize the plumbing so that sources and sinks are as close to each other as possible. \square

We have seen how the probability of a single \mathbf{S} surviving at the end of the circuit at one location is related to the feedforward distance. Let us also study the case $\Pr[\vec{x}_A^d = 11\dots1]$, the probability of ending up with the all \mathbf{S} operator on a region A .

Lemma 11. For a region A , the probability that the final bitstring contains $\mathbf{S}\dots\mathbf{S}$ in the entire region A , i.e. $\Pr_{\mathcal{X}_d}[\vec{x}_l^d = 1 \forall l \in A]$, is lower bounded by

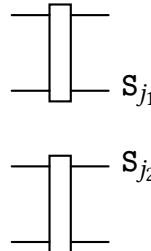
$$\left(\frac{\sin^2 \varphi}{3}\right)^{|A|} \left(\frac{\alpha}{5}\right)^{\sum_{i \in A} |p(\ell(t_i), i)|} \quad (100)$$

for any set of paths starting from some feedforward operation t_i and ending at sites in A $\ell(d_i) = i$.

Proof. For every qubit in A , consider the path with shortest path length to a nearby feedforward operation in the circuit \mathcal{C} . For two distinct qubits, it is possible that the shortest paths overlap significantly and begin at the same feedforward operation.

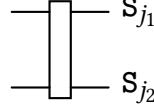
One may apply Lemma 10 to bound the mass of each $\mathbf{S}_{i \in A}$ separately. The events are not independent because multiple paths from the same source could contribute to the event of seeing an $\mathbf{S}\dots\mathbf{S}_A$ string at the output. But this can be handled since the events are positively correlated ($\Pr[\vec{x}_{j_1}^i = 1 \& \vec{x}_{j_2}^i = 1 | E] \geq \Pr[\vec{x}_{j_1}^i = 1 | E] \cdot \Pr[\vec{x}_{j_2}^i = 1 | E]$) for some prior event E that both events condition upon. The fact that the correlation is positive can be checked case by case, but intuitively it follows from the fact that our lower bound on the event that an \mathbf{S} at a site survives, $\Pr[\mathbf{S}_j = 1 | \mathbf{S}_j = 1] \geq \frac{\alpha}{5}$, actually corresponds to an event where the \mathbf{S} duplicates on to another site: $\mathbf{S}\mathbf{S}$. Consider a pair of sites j_1 and j_2 and let us prove the positive correlation.

Case i). In this case there is no gate between these qubits in the layer preceding them and there is no common qubit in their backwards light cone of depth 1:



Here, the probability $\Pr[\vec{x}_{j_1}^i = 1 \& \vec{x}_{j_2}^i = 1 | E]$ equals $\Pr[\vec{x}_{j_1}^i = 1 | E] \cdot \Pr[\vec{x}_{j_2}^i = 1 | E]$ because the events are independent.

Case ii). In this case there is a gate between the qubits in the preceding layer.



If the input is $\vec{x}_{j_1, j_2}^{i-1} = 11$, then we have $\Pr[\mathbf{SS}|\mathbf{SS}] = 1$, which equals $\Pr[\mathbf{S}_{j_1}|\mathbf{SS}] \cdot \Pr[\mathbf{S}_{j_2}|\mathbf{SS}]$. Similarly, if the input is $\vec{x}_{j_1, j_2}^{i-1} = 00$, then $\Pr[\mathbf{SS}|\mathbf{II}] = 0 = \Pr[\mathbf{S}_{j_1}|\mathbf{II}] \cdot \Pr[\mathbf{S}_{j_2}|\mathbf{II}]$. The last two cases, which are symmetric, are $\Pr[\mathbf{SS}|\mathbf{IS} \text{ or } \mathbf{SI}]$. Considering one of these,

$$\Pr[\mathbf{SS}|\mathbf{IS}] = \frac{\alpha}{5} \geq \Pr[\mathbf{S}_{j_1}|\mathbf{IS}] \cdot \Pr[\mathbf{S}_{j_2}|\mathbf{IS}] = \left(\frac{\alpha}{5}\right)^2. \quad (101)$$

Therefore, we can lower bound the event by assuming conditional independence, giving

$$\left(\frac{\sin^2 \varphi}{3}\right)^{n_t} \left(\frac{\alpha}{5}\right)^{\sum_{i \in A} |p(\ell(t_i), i)|}, \quad (102)$$

where n_t is the number of sources \mathbf{S} strings. In the worst case, each \mathbf{S} string comes from a different source giving $n_t = |A|$ the locality of A . The entire lower bound is now

$$\Pr_{\mathcal{X}_d^d}[\vec{x}_l^d = 1 \forall l \in A] \geq \left(\frac{\sin^2 \varphi}{3}\right)^{|A|} \left(\frac{\alpha}{5}\right)^{\sum_{i \in A} |p(\ell(t_i), i)|}. \quad (103)$$

The quantity in the exponent is obtained by independently choosing a path for every qubit in A . \square

We are ready to prove our main result on the absence of barren plateaus.

Theorem 12. Consider a k -local Hermitian observable $H = \sum_{\alpha} c_{\alpha} \alpha$, and a parameterized dynamic quantum circuit \mathcal{C} , with parameters $\theta \in \Theta$, that satisfies the following properties:

1. Every component $\theta_i \in \theta$ parameterizes only a single operation in \mathcal{C} .
2. \mathcal{C} is invariant under single-qubit random gates from a 2-design after every gate
3. The distribution over two-qubit gates has a transfer matrix of the form Eq. (50).
4. \mathcal{C} has constant worst-case feedforward distance f .

Then, the variance of the loss function $L = \text{Tr } \rho(\theta)H$ is lower bounded by

$$\text{Var } L_{\theta \sim \mathcal{D}_p} \geq \sum_{\alpha} c_{\alpha}^2 \left(\frac{\sin^2 \varphi}{3}\right)^{|\alpha|} \left(\frac{\alpha}{5}\right)^{kf}. \quad (104)$$

Proof. Consider a circuit architecture such that the worst-case feedforward distance, f is upper bounded by a constant. Assume the loss function is $\sum_{\alpha \in \mathbb{P}_n} c_{\alpha} \alpha$ expanded in the Pauli basis. We may ignore the identity term since it does not contribute to the variance. Since the maximum locality of the Hamiltonian is k , so too is the maximum weight of any Pauli. Since the worst-case feedforward distance is the maximum feedforward distance among any qubit at the output, in the worst case, the sum $\sum_{i \in A} |p(\ell(t_i), i)|$ is at most $f \times k$. The rest follows from Lemmas 5 and 11. \square

Further fixing an architecture where f is constant and $\varphi = \pi/2$, we get a lower bound on the variance of the form

$$\sum_{\alpha} c_{\alpha}^2 \cdot \Omega(1) = \Omega(\|H\|_{HS}^2), \quad (105)$$

where $\|H\|_{HS} := \sqrt{\frac{\text{Tr } H^2}{2^n}}$ is the Hilbert-Schmidt norm of the operator H .

We can also prove the robustness of this result to unital noise:

Theorem 13. Consider a k -local Hermitian observable $H = \sum_{\alpha} c_{\alpha} \alpha$, and a parameterized dynamic quantum circuit \mathcal{C} , with parameters $\theta \in \Theta$, that satisfies the following properties:

1. Every component $\theta_i \in \theta$ parameterizes only a single operation in \mathcal{C} .
2. \mathcal{C} is invariant under single-qubit random gates from a 2-design after every gate.
3. The distribution over two-qubit gates has a transfer matrix of the form Eq. (50).
4. \mathcal{C} has constant worst-case feedforward distance f .
5. Assume that after every two-qubit operation, there is some unital local noise acting on every qubit with a transfer matrix given in Eq. (54).

Then, the variance of the loss function $L = \text{Tr } \rho(\theta)H$ is lower bounded by

$$\text{Var } L_{\theta \sim \mathcal{D}_p} \geq \sum_{\alpha} c_{\alpha}^2 \left(\frac{\sin^2 \varphi}{3} \right)^{|\alpha|} \left(\frac{\alpha(1-\gamma)^2}{5} \right)^{kf}. \quad (106)$$

Proof. We observe that under unital noise, the combined transfer matrix of the two-qubit gate and the noise channel becomes

$$T = \begin{pmatrix} 1 & (1-\gamma)\frac{(4-\gamma)}{5} + \gamma & (1-\gamma)\frac{(4-\gamma)}{5} & \gamma^2 \\ 0 & (1-\gamma)(1-\alpha-\beta + \frac{\alpha\gamma}{5}) & (1-\gamma)(\beta + \frac{\alpha\gamma}{5}) & \gamma(1-\gamma) \\ 0 & (1-\gamma)(\beta + \frac{\alpha\gamma}{5}) & (1-\gamma)(1-\alpha-\beta + \frac{\alpha\gamma}{5}) & \gamma(1-\gamma) \\ 0 & \frac{\alpha}{5}(1-\gamma)^2 & \frac{\alpha}{5}(1-\gamma)^2 & (1-\gamma)^2 \end{pmatrix}. \quad (107)$$

We observe that the appropriate part of the proof above is the lower bound on the probability that an S survives. Thus, we can make the replacement $\frac{\alpha}{5} \rightarrow \frac{\alpha}{5}(1-\gamma)^2$ in the proof and obtain the modified lower bound. \square

References

- [ABIN96] D. Aharonov, M. Ben-Or, R. Impagliazzo, and N. Nisan. “Limitations of Noisy Reversible Computation” (1996). arXiv: [quant-ph/9611028](#).
- [Aha+22] Dorit Aharonov, Xun Gao, Zeph Landau, Yunchao Liu, and Umesh Vazirani. “A Polynomial-Time Classical Algorithm for Noisy Random Circuit Sampling”. arXiv:2211.03999 (2022). arXiv: [2211.03999 \[quant-ph\]](#).
- [AHCC22] Andrew Arrasmith, Zoë Holmes, M Cerezo, and Patrick J Coles. “Equivalence of Quantum Barren Plateaus to Cost Concentration and Narrow Gorges”. *Quantum Science and Technology* 7.4 (2022), p. 045015. doi: [10.1088/2058-9565/ac7d06](#).
- [Ang+24] Armando Angrisani, Alexander Schmidhuber, Manuel S. Rudolph, M. Cerezo, Zoë Holmes, and Hsin-Yuan Huang. “Classically Estimating Observables of Noiseless Quantum Circuits”. arXiv:2409.01706 (2024). arXiv: [2409.01706 \[math-ph, physics:quant-ph\]](#).
- [Bäu+24a] Elisa Bäumer, Vinay Tripathi, Alireza Seif, Daniel Lidar, and Derek S. Wang. “Quantum Fourier Transform Using Dynamic Circuits”. arXiv:2403.09514 (2024). arXiv: [2403.09514 \[quant-ph\]](#).
- [Bäu+24b] Elisa Bäumer, Vinay Tripathi, Derek S. Wang, Patrick Rall, Edward H. Chen, Swarnadeep Majumder, Alireza Seif, and Zlatko K. Minev. “Efficient Long-Range Entanglement Using Dynamic Circuits”. *PRX Quantum* 5.3 (2024), p. 030339. doi: [10.1103/PRXQuantum.5.030339](#).
- [Bee+20] Kerstin Beer, Dmytro Bondarenko, Terry Farrelly, Tobias J. Osborne, Robert Salzmann, Daniel Scheiermann, and Ramona Wolf. “Training Deep Quantum Neural Networks”. *Nature Communications* 11.1 (2020), p. 808. doi: [10.1038/s41467-020-14454-2](#).

[BF20] Dmytro Bondarenko and Polina Feldmann. “Quantum Autoencoders to Denoise Quantum Data”. *Physical Review Letters* 124.13 (2020), p. 130502. doi: [10.1103/PhysRevLett.124.130502](https://doi.org/10.1103/PhysRevLett.124.130502).

[BFLN23] Harry Buhrman, Marten Folkertsma, Bruno Loff, and Niels M. P. Neumann. “State Preparation by Shallow Circuits Using Feed Forward”. arXiv:2307.14840 (2023). doi: [10.48550/arXiv.2307.14840](https://doi.org/10.48550/arXiv.2307.14840).

[BGH13] Michael Ben-Or, Daniel Gottesman, and Avinatan Hassidim. “Quantum Refrigerator” (2013). arXiv: [1301.1995 \[quant-ph\]](https://arxiv.org/abs/1301.1995).

[BKKK22] Sergey Bravyi, Isaac Kim, Alexander Kliesch, and Robert Koenig. “Adaptive Constant-Depth Circuits for Manipulating Non-Abelian Anyons”. arXiv:2205.01933 (2022). arXiv: [2205.01933 \[quant-ph\]](https://arxiv.org/abs/2205.01933).

[BLSF19] Marcello Benedetti, Erika Lloyd, Stefan Sack, and Mattia Fiorentini. “Parameterized quantum circuits as machine learning models”. *Quantum Science and Technology* 4.4 (Nov. 2019), p. 043001. issn: 2058-9565. doi: [10.1088/2058-9565/ab4eb5](https://doi.org/10.1088/2058-9565/ab4eb5). URL: <http://dx.doi.org/10.1088/2058-9565/ab4eb5>.

[BM21] Kerstin Beer and Gabriel Müller. “Dissipative Quantum Generative Adversarial Networks”. arXiv:2112.06088 (2021). arXiv: [2112.06088 \[quant-ph\]](https://arxiv.org/abs/2112.06088).

[Bri+09] H. J. Briegel, D. E. Browne, W. Dür, R. Raussendorf, and M. Van den Nest. “Measurement-Based Quantum Computation”. *Nature Physics* 5.1 (2009), pp. 19–26. doi: [10.1038/nphys1157](https://doi.org/10.1038/nphys1157).

[BW24] Elisa Bäumer and Stefan Woerner. “Measurement-Based Long-Range Entangling Gates in Constant Depth”. arXiv:2408.03064 (2024). arXiv: [2408.03064 \[quant-ph\]](https://arxiv.org/abs/2408.03064).

[Car+23] Matthias C. Caro, Hsin-Yuan Huang, Nicholas Ezzell, Joe Gibbs, Andrew T. Sornborger, Lukasz Cincio, Patrick J. Coles, and Zoë Holmes. “Out-of-distribution generalization for learning quantum dynamics”. *Nature Communications* 14.1 (July 2023). issn: 2041-1723. doi: [10.1038/s41467-023-39381-w](https://doi.org/10.1038/s41467-023-39381-w). URL: <http://dx.doi.org/10.1038/s41467-023-39381-w>.

[CC21] M Cerezo and Patrick J Coles. “Higher Order Derivatives of Quantum Neural Networks with Barren Plateaus”. *Quantum Science and Technology* 6.3 (2021), p. 035006. doi: [10.1088/2058-9565/abf51a](https://doi.org/10.1088/2058-9565/abf51a).

[CCL19] Iris Cong, Soonwon Choi, and Mikhail D. Lukin. “Quantum Convolutional Neural Networks”. *Nature Physics* 15.12 (2019), pp. 1273–1278. doi: [10.1038/s41567-019-0648-8](https://doi.org/10.1038/s41567-019-0648-8).

[Cer+21a] M. Cerezo, Andrew Arrasmith, Ryan Babbush, Simon C. Benjamin, Suguru Endo, Keisuke Fujii, Jarrod R. McClean, Kosuke Mitarai, Xiao Yuan, Lukasz Cincio, and Patrick J. Coles. “Variational quantum algorithms”. *Nature Reviews Physics* 3.9 (Aug. 2021), pp. 625–644. issn: 2522-5820. doi: [10.1038/s42254-021-00348-9](https://doi.org/10.1038/s42254-021-00348-9). URL: <http://dx.doi.org/10.1038/s42254-021-00348-9>.

[Cer+21b] M. Cerezo, Akira Sone, Tyler Volkoff, Lukasz Cincio, and Patrick J. Coles. “Cost Function Dependent Barren Plateaus in Shallow Parametrized Quantum Circuits”. *Nature Communications* 12.1 (2021), p. 1791. doi: [10.1038/s41467-021-21728-w](https://doi.org/10.1038/s41467-021-21728-w).

[Cer+23] M. Cerezo, Martin Larocca, Diego García-Martín, N. L. Diaz, Paolo Braccia, Enrico Fontana, Manuel S. Rudolph, Pablo Bermejo, Aroosa Ijaz, Supanut Thanasilp, Eric R. Anschuetz, and Zoë Holmes. “Does Provable Absence of Barren Plateaus Imply Classical Simulability? Or, Why We Need to Rethink Variational Quantum Computing”. arXiv:2312.09121 (2023). doi: [10.48550/arXiv.2312.09121](https://doi.org/10.48550/arXiv.2312.09121).

[Cór+21] A. D. Córcoles, Maika Takita, Ken Inoue, Scott Lekuch, Zlatko K. Minev, Jerry M. Chow, and Jay M. Gambetta. “Exploiting Dynamic Quantum Circuits in a Quantum Algorithm with Superconducting Qubits”. *Physical Review Letters* 127.10 (2021), p. 100501. doi: [10.1103/PhysRevLett.127.100501](https://doi.org/10.1103/PhysRevLett.127.100501).

[Des+22] Abhinav Deshpande, Pradeep Niroula, Oles Shtanko, Alexey V. Gorshkov, Bill Fefferman, and Michael J. Gullans. “Tight Bounds on the Convergence of Noisy Random Circuits to the Uniform Distribution”. *PRX Quantum* 3.4 (2022), p. 040329. doi: [10.1103/PRXQuantum.3.040329](https://doi.org/10.1103/PRXQuantum.3.040329).

[DHB20] Alexander M. Dalzell, Nicholas Hunter-Jones, and Fernando G. S. L. Brandão. “Random Quantum Circuits Anti-Concentrate in Log Depth” (2020). arXiv: [2011.12277](https://arxiv.org/abs/2011.12277) [cond-mat, physics:quant-ph].

[DHB21] Alexander M. Dalzell, Nicholas Hunter-Jones, and Fernando G. S. L. Brandão. “Random Quantum Circuits Transform Local Noise into Global White Noise” (2021). arXiv: [2111.14907](https://arxiv.org/abs/2111.14907) [quant-ph].

[Fon+23] Enrico Fontana, Manuel S. Rudolph, Ross Duncan, Ivan Rungger, and Cristina Cîrstoiu. “Classical Simulations of Noisy Variational Quantum Circuits”. arXiv:2306.05400 (2023). arXiv: [2306.05400](https://arxiv.org/abs/2306.05400) [quant-ph].

[Fos+23] Michael Foss-Feig, Arkin Tikku, Tsung-Cheng Lu, Karl Mayer, Mohsin Iqbal, Thomas M. Gatterman, Justin A. Gerber, Kevin Gilmore, Dan Gresh, Aaron Hankin, Nathan Hewitt, Chandler V. Horst, Mitchell Matheny, Tanner Mengle, Brian Neyenhuis, Henrik Dreyer, David Hayes, Timothy H. Hsieh, and Isaac H. Kim. “Experimental Demonstration of the Advantage of Adaptive Quantum Circuits”. arXiv:2302.03029 (2023). arXiv: [2302.03029](https://arxiv.org/abs/2302.03029) [cond-mat, physics:quant-ph].

[GD18] Xun Gao and Luming Duan. “Efficient Classical Simulation of Noisy Quantum Computation” (2018). arXiv: [1810.03176](https://arxiv.org/abs/1810.03176) [quant-ph].

[GGPD24] Elies Gil-Fuster, Casper Gyurik, Adrián Pérez-Salinas, and Vedran Dunjko. “On the Relation between Trainability and Dequantization of Variational Quantum Learning Models”. arXiv:2406.07072 (2024). arXiv: [2406.07072](https://arxiv.org/abs/2406.07072) [quant-ph, stat].

[GSV16] Andreas Galanis, Daniel Stefankovic, and Eric Vigoda. “Inapproximability of the Partition Function for the Antiferromagnetic Ising and Hard-Core Models”. *Combinatorics, Probability and Computing* 25.4 (2016), pp. 500–559. doi: [10.1017/S0963548315000401](https://doi.org/10.1017/S0963548315000401).

[GWOB19] Edward Grant, Leonard Wossnig, Mateusz Ostaszewski, and Marcello Benedetti. “An Initialization Strategy for Addressing Barren Plateaus in Parametrized Quantum Circuits”. *Quantum* 3 (2019), p. 214. doi: [10.22331/q-2019-12-09-214](https://doi.org/10.22331/q-2019-12-09-214).

[HSCC22] Zoë Holmes, Kunal Sharma, M. Cerezo, and Patrick J. Coles. “Connecting Ansatz Expressibility to Gradient Magnitudes and Barren Plateaus”. *PRX Quantum* 3.1 (2022), p. 345. doi: [10.1103/PRXQuantum.3.010313](https://doi.org/10.1103/PRXQuantum.3.010313).

[Hun19] Nicholas Hunter-Jones. “Unitary Designs from Statistical Mechanics in Random Quantum Circuits” (2019). arXiv: [1905.12053](https://arxiv.org/abs/1905.12053) [cond-mat, physics:hep-th, physics:quant-ph].

[IA24] Yigal Ilin and Itai Arad. “Dissipative Variational Quantum Algorithms for Gibbs State Preparation”. arXiv:2407.09635 (2024). doi: [10.48550/arXiv.2407.09635](https://doi.org/10.48550/arXiv.2407.09635).

[KB15] Diederik P. Kingma and Jimmy Ba. “Adam: A Method for Stochastic Optimization”. *3rd International Conference on Learning Representations*. Ed. by Yoshua Bengio and Yann LeCun. 2015.

[KSS92] Michael J. Kearns, Robert E. Schapire, and Linda M. Sellie. “Toward efficient agnostic learning”. *Proceedings of the Fifth Annual Workshop on Computational Learning Theory*. COLT ’92. Pittsburgh, Pennsylvania, USA: Association for Computing Machinery, 1992, pp. 341–352. ISBN: 089791497X. doi: [10.1145/130385.130424](https://doi.org/10.1145/130385.130424). url: <https://doi.org/10.1145/130385.130424>.

[Lar+24] Martin Larocca, Supanut Thanasilp, Samson Wang, Kunal Sharma, Jacob Biamonte, Patrick J. Coles, Lukasz Cincio, Jarrod R. McClean, Zoë Holmes, and M. Cerezo. “A Review of Barren Plateaus in Variational Quantum Computing”. arXiv:2405.00781 (2024). doi: [10.48550/arXiv.2405.00781](https://doi.org/10.48550/arXiv.2405.00781).

[Li+23] Yabo Li, Hiroki Sukeno, Aswin Parayil Mana, Hendrik Poulsen Nautrup, and Tzu-Chieh Wei. “Symmetry-Enriched Topological Order from Partially Gauging Symmetry-Protected Topologically Ordered States Assisted by Measurements”. *Physical Review B* 108.11 (2023), p. 115144. doi: [10.1103/PhysRevB.108.115144](https://doi.org/10.1103/PhysRevB.108.115144).

[LLKH22] Tsung-Cheng Lu, Leonardo A. Lessa, Isaac H. Kim, and Timothy H. Hsieh. “Measurement as a Shortcut to Long-Range Entangled Quantum Matter”. *PRX Quantum* 3.4 (2022), p. 040337. doi: [10.1103/PRXQuantum.3.040337](https://doi.org/10.1103/PRXQuantum.3.040337).

[LWZ24] Alistair Letcher, Stefan Woerner, and Christa Zoufal. “Tight and Efficient Gradient Bounds for Parameterized Quantum Circuits”. arXiv:2309.12681 (2024). arXiv: [2309.12681 \[quant-ph\]](https://arxiv.org/abs/2309.12681).

[McC+18] Jarrod R. McClean, Sergio Boixo, Vadim N. Smelyanskiy, Ryan Babbush, and Hartmut Neven. “Barren Plateaus in Quantum Neural Network Training Landscapes”. *Nature Communications* 9.1 (2018), p. 4812. doi: [10.1038/s41467-018-07090-4](https://doi.org/10.1038/s41467-018-07090-4).

[Mel+24] Antonio Anna Mele, Armando Angrisani, Soumik Ghosh, Sumeet Khatri, Jens Eisert, Daniel Stilck França, and Yihui Quek. “Noise-Induced Shallow Circuits and Absence of Barren Plateaus”. arXiv:2403.13927 (2024). arXiv: [2403.13927 \[cond-mat, physics:math-ph, physics:quant-ph\]](https://arxiv.org/abs/2403.13927).

[MNKF18] Kosuke Mitarai, Makoto Negoro, Masahiro Kitagawa, and Keisuke Fujii. “Quantum circuit learning”. *Physical Review A* 98.3 (2018), p. 032309.

[MSWC24] Daniel Malz, Georgios Styliaris, Zhi-Yuan Wei, and J. Ignacio Cirac. “Preparation of Matrix Product States with Log-Depth Quantum Circuits”. *Physical Review Letters* 132.4 (2024), p. 040404. doi: [10.1103/PhysRevLett.132.040404](https://doi.org/10.1103/PhysRevLett.132.040404).

[Nap22] John Napp. “Quantifying the Barren Plateau Phenomenon for a Model of Unstructured Variational Ansätze”. arXiv:2203.06174 (2022). arXiv: [2203.06174 \[quant-ph\]](https://arxiv.org/abs/2203.06174).

[Nie23] Alexander Nietner. “Unifying (Quantum) Statistical and Parametrized (Quantum) Algorithms”. arXiv:2310.17716 (2023). arXiv: [2310.17716 \[quant-ph, stat\]](https://arxiv.org/abs/2310.17716).

[OKW21] Carlos Ortiz Marrero, Mária Kieferová, and Nathan Wiebe. “Entanglement-Induced Barren Plateaus”. *PRX Quantum* 2.4 (2021), p. 040316. doi: [10.1103/PRXQuantum.2.040316](https://doi.org/10.1103/PRXQuantum.2.040316).

[PBO20] Kyle Poland, Kerstin Beer, and Tobias J. Osborne. “No Free Lunch for Quantum Machine Learning”. arXiv:2003.14103 (2020). arXiv: [2003.14103 \[quant-ph\]](https://arxiv.org/abs/2003.14103).

[Pes+21] Arthur Pesah, M. Cerezo, Samson Wang, Tyler Volkoff, Andrew T. Sornborger, and Patrick J. Coles. “Absence of Barren Plateaus in Quantum Convolutional Neural Networks”. *Physical Review X* 11.4 (2021), p. 041011. doi: [10.1103/PhysRevX.11.041011](https://doi.org/10.1103/PhysRevX.11.041011).

[PSC21] Lorenzo Piroli, Georgios Styliaris, and J. Ignacio Cirac. “Quantum Circuits Assisted by Local Operations and Classical Communication: Transformations and Phases of Matter”. *Physical Review Letters* 127.22 (2021). doi: [10.1103/physrevlett.127.220503](https://doi.org/10.1103/physrevlett.127.220503).

[PSC24] Lorenzo Piroli, Georgios Styliaris, and J. Ignacio Cirac. “Approximating Many-Body Quantum States with Quantum Circuits and Measurements”. arXiv:2403.07604 (2024). arXiv: [2403.07604 \[cond-mat, physics:quant-ph\]](https://arxiv.org/abs/2403.07604).

[RMM+23] Manuel S. Rudolph, Jacob Miller, Danial Motlagh, et al. “Synergistic Pretraining of Parametrized Quantum Circuits via Tensor Networks”. *Nature Communications* 14.1 (2023), p. 8367. doi: [10.1038/s41467-023-43908-6](https://doi.org/10.1038/s41467-023-43908-6).

[SCCC22] Kunal Sharma, M. Cerezo, Lukasz Cincio, and Patrick J. Coles. “Trainability of Dissipative Perceptron-Based Quantum Neural Networks”. *Physical Review Letters* 128.18 (2022). doi: [10.1103/physrevlett.128.180505](https://doi.org/10.1103/physrevlett.128.180505).

[Sch+19] Maria Schuld, Ville Bergholm, Christian Gogolin, Josh Izaac, and Nathan Killoran. “Evaluating analytic gradients on quantum hardware”. *Physical Review A* 99.3 (2019), p. 032331.

[SKCC20] Kunal Sharma, Sumeet Khatri, M. Cerezo, and Patrick J. Coles. “Noise Resilience of Variational Quantum Compiling”. *New Journal of Physics* 22.4 (2020), p. 043006. doi: [10.1088/1367-2630/ab784c](https://doi.org/10.1088/1367-2630/ab784c).

[Smi+24] Kevin C. Smith, Abid Khan, Bryan K. Clark, S.M. Girvin, and Tzu-Chieh Wei. “Constant-Depth Preparation of Matrix Product States with Adaptive Quantum Circuits”. *PRX Quantum* 5.3 (2024), p. 030344. doi: [10.1103/PRXQuantum.5.030344](https://doi.org/10.1103/PRXQuantum.5.030344).

[Son+24] Yongxin Song, Liberto Beltrán, Ilya Besedin, Michael Kerschbaum, Marek Pechal, François Swiadek, Christoph Hellings, Dante Colao Zanuz, Alexander Flasby, Jean-Claude Besse, and Andreas Wallraff. “Realization of Constant-Depth Fan-Out with Real-Time Feedforward on a Superconducting Quantum Processor”. arXiv:2409.06989 (2024). arXiv: [2409.06989 \[quant-ph\]](https://arxiv.org/abs/2409.06989).

[SWCL23] Yuguo Shao, Fuchuan Wei, Song Cheng, and Zhengwei Liu. “Simulating Quantum Mean Values in Noisy Variational Quantum Algorithms: A Polynomial-Scale Approach”. arXiv:2306.05800 (2023). arXiv: [2306.05804 \[quant-ph\]](https://arxiv.org/abs/2306.05804).

[SYGY24] Thomas Schuster, Chao Yin, Xun Gao, and Norman Y. Yao. “A Polynomial-Time Classical Algorithm for Noisy Quantum Circuits”. arXiv:2407.12768 (2024). arXiv: [2407.12768 \[math-ph, physics:physics, physics:quant-ph\]](https://arxiv.org/abs/2407.12768).

[Til+22] Jules Tilly, Hongxiang Chen, Shuxiang Cao, Dario Picozzi, Kanav Setia, Ying Li, Edward Grant, Leonard Wossnig, Ivan Rungger, George H. Booth, and Jonathan Tennyson. “The Variational Quantum Eigensolver: A review of methods and best practices”. *Physics Reports* 986 (Nov. 2022), pp. 1–128. ISSN: 0370-1573. doi: [10.1016/j.physrep.2022.08.003](https://doi.org/10.1016/j.physrep.2022.08.003). URL: <http://dx.doi.org/10.1016/j.physrep.2022.08.003>.

[TVV23a] Nathanan Tantivasadakarn, Ruben Verresen, and Ashvin Vishwanath. “Shortest Route to Non-Abelian Topological Order on a Quantum Processor”. *Physical Review Letters* 131.6 (2023), p. 060405. doi: [10.1103/PhysRevLett.131.060405](https://doi.org/10.1103/PhysRevLett.131.060405).

[TVV23b] Nathanan Tantivasadakarn, Ashvin Vishwanath, and Ruben Verresen. “Hierarchy of Topological Order From Finite-Depth Unitaries, Measurement, and Feedforward”. *PRX Quantum* 4.2 (2023), p. 020339. doi: [10.1103/PRXQuantum.4.020339](https://doi.org/10.1103/PRXQuantum.4.020339).

[UB21] Alexey Uvarov and Jacob Biamonte. “On Barren Plateaus and Cost Function Locality in Variational Quantum Algorithms”. *Journal of Physics A: Mathematical and Theoretical* 54.24 (2021), p. 245301. doi: [10.1088/1751-8121/abfac7](https://doi.org/10.1088/1751-8121/abfac7).

[VTB22] Ruben Verresen, Nathanan Tantivasadakarn, and Ashvin Vishwanath. “Efficiently Preparing Schrödinger’s Cat, Fractons and Non-Abelian Topological Order in Quantum Devices”. arXiv:2112.03061 (2022). arXiv: [2112.03061 \[cond-mat, physics:physics, physics:quant-ph\]](https://arxiv.org/abs/2112.03061).

[Wan+21] Samson Wang, Enrico Fontana, M. Cerezo, Kunal Sharma, Akira Sone, Lukasz Cincio, and Patrick J. Coles. “Noise-Induced Barren Plateaus in Variational Quantum Algorithms”. *Nature Communications* 12.1 (2021), p. 6961. doi: [10.1038/s41467-021-27045-6](https://doi.org/10.1038/s41467-021-27045-6).

[War+23] Brayden Ware, Abhinav Deshpande, Dominik Hangleiter, Pradeep Niroula, Bill Fefferman, Alexey V. Gorshkov, and Michael J. Gullans. “A Sharp Phase Transition in Linear Cross-Entropy Benchmarking”. arXiv:2305.04954 (2023). arXiv: [2305.04954](https://arxiv.org/abs/2305.04954) [cond-mat, physics:quant-ph].

[WIWL22] David Wierichs, Josh Izaac, Cody Wang, and Cedric Yen-Yu Lin. “General parameter-shift rules for quantum gradients”. *Quantum* 6 (Mar. 2022), p. 677. issn: 2521-327X. doi: [10.22331/q-2022-03-30-677](https://doi.org/10.22331/q-2022-03-30-677). URL: <http://dx.doi.org/10.22331/q-2022-03-30-677>.

[WLW21] Youle Wang, Guangxi Li, and Xin Wang. “Variational Quantum Gibbs State Preparation with a Truncated Taylor Series”. *Phys. Rev. Appl.* 16 (5 Nov. 2021), p. 054035. doi: [10.1103/PhysRevApplied.16.054035](https://doi.org/10.1103/PhysRevApplied.16.054035). URL: <https://link.aps.org/doi/10.1103/PhysRevApplied.16.054035>.

[WQFD23] Yabo Wang, Bo Qi, Chris Ferrie, and Daoyi Dong. “Trainability Enhancement of Parameterized Quantum Circuits via Reduced-Domain Parameter Initialization”. arXiv:2302.06858 (2023). arXiv: [2302.06858](https://arxiv.org/abs/2302.06858) [quant-ph].

[WSB03] Xiaoguang Wang, Barry C. Sanders, and Dominic W. Berry. “Entangling Power and Operator Entanglement in Qudit Systems”. *Physical Review A* 67.4 (2003), p. 042323. doi: [10.1103/PhysRevA.67.042323](https://doi.org/10.1103/PhysRevA.67.042323).

[YMZM24] Yuxuan Yan, Muzhou Ma, You Zhou, and Xiongfeng Ma. “Variational LOCC-assisted Quantum Circuits for Long-Range Entangled States”. arXiv:2409.07281 (2024). arXiv: [2409.07281](https://arxiv.org/abs/2409.07281) [quant-ph].

[Zha+23] Shi-Xin Zhang, Jonathan Allcock, Zhou-Quan Wan, Shuo Liu, Jiace Sun, Hao Yu, Xing-Han Yang, Jiezhong Qiu, Zhaofeng Ye, Yu-Qin Chen, Chee-Kong Lee, Yi-Cong Zheng, Shao-Kai Jian, Hong Yao, Chang-Yu Hsieh, and Shengyu Zhang. “TensorCircuit: a Quantum Software Framework for the NISQ Era”. *Quantum* 7 (Feb. 2023), p. 912. issn: 2521-327X. doi: [10.22331/q-2023-02-02-912](https://doi.org/10.22331/q-2023-02-02-912). URL: <https://doi.org/10.22331/q-2023-02-02-912>.

[Zho+20] Leo Zhou, Sheng-Tao Wang, Soonwon Choi, Hannes Pichler, and Mikhail D. Lukin. “Quantum Approximate Optimization Algorithm: Performance, Mechanism, and Implementation on Near-Term Devices”. *Physical Review X* 10.2 (June 2020). issn: 2160-3308. doi: [10.1103/physrevx.10.021067](https://doi.org/10.1103/physrevx.10.021067). URL: <http://dx.doi.org/10.1103/PhysRevX.10.021067>.

[ZLHT22] Kaining Zhang, Liu Liu, Min-Hsiu Hsieh, and Dacheng Tao. “Escaping from the Barren Plateau via Gaussian Initializations in Deep Variational Quantum Circuits”. *Advances in Neural Information Processing Systems*. Ed. by Alice H. Oh, Alekh Agarwal, Danielle Belgrave, and Kyunghyun Cho. Vol. 35. 2022.

[ZLW21] Christa Zoufal, Aurélien Lucchi, and Stefan Woerner. “Variational quantum Boltzmann machines”. *Quantum Machine Intelligence* 3.1 (2021), p. 7. doi: [10.1007/s42484-020-00033-7](https://doi.org/10.1007/s42484-020-00033-7). URL: <https://doi.org/10.1007/s42484-020-00033-7>.

[ZLZ24] Hao-Kai Zhang, Shuo Liu, and Shi-Xin Zhang. “Absence of Barren Plateaus in Finite Local-Depth Circuits with Long-Range Entanglement”. *Physical Review Letters* (2024).

[ZZF00] Paolo Zanardi, Christof Zalka, and Lara Faoro. “Entangling Power of Quantum Evolutions”. *Physical Review A* 62.3 (2000), p. 030301. doi: [10.1103/PhysRevA.62.030301](https://doi.org/10.1103/PhysRevA.62.030301).